CHALMERS
UNIVERSITY OF TECHNOLOGY

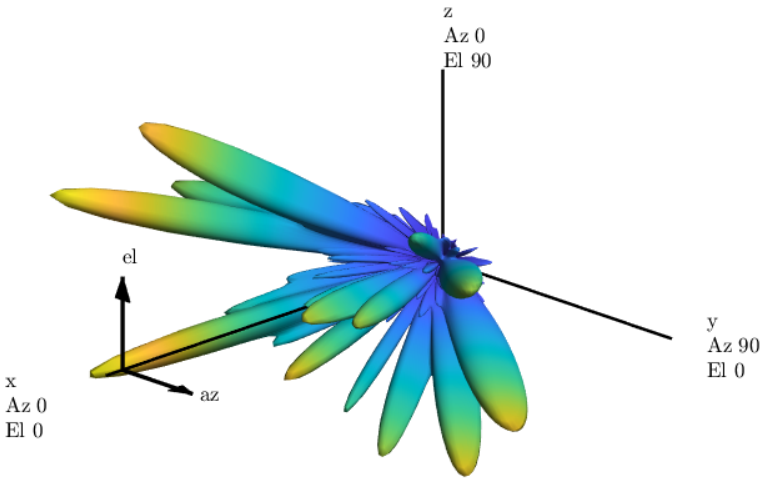

Hybrid Beamforming for Future mm-Wave Access in Mobile Communication

Beamforming Weight Algorithms and Hardware Investigations

Master's thesis in Wireless, Photonics and Space Engineering

ISABEL VRETHED TIDEKRANS

Department of Electrical Engineering
CHALMERS UNIVERSITY OF TECHNOLOGY
Gothenburg, Sweden 2020

Master's thesis 2020:XX

Hybrid Beamforming for Future mm-Wave Access in Mobile Communication

Beamforming Weight Algorithms and Hardware Investigations

ISABEL VRETHED TIDEKRANS

CHALMERS
UNIVERSITY OF TECHNOLOGY

Department of Electrical Engineering
Chalmers University of Technology
Gothenburg, Sweden 2020

Hybrid Beamforming for Future mm-Wave Access in Mobile Communication
Beamforming Weight Algorithms and Hardware Investigations
ISABEL VRETHED TIDEKRANS

Company supervisor: Johan Wettergren, Qamcom Research & Technology
Supervisor: Ahmet Oguz Kislal, Department of Electrical Engineering
Examiner: Thomas Eriksson, Department of Electrical Engineering

Master's Thesis 2020:XX
Department of Electrical Engineering
Chalmers University of Technology
SE-412 96 Gothenburg
Telephone +46 (0)31-772 10 00

Cover: Visualization of radiation pattern from a transmitter with a square 256 element antenna array using optimal hybrid beamforming weights.

Typeset in LaTeX
Printed by Chalmers Reproservice
Gothenburg, Sweden 2020

Hybrid Beamforming for Future mm-Wave Access in Mobile Communication
Beamforming weight algorithms and hardware investigations
ISABEL VRETHED TIDEKRANS
Department of Electrical Engineering
Chalmers University of Technology

Abstract

Hybrid beamforming solutions have been investigated at 28 GHz for a base station equipped with many antennas, transmitting to one or multiple users with multiple antennas each. Hybrid beamforming utilizes several RF chains, and a larger amount of antennas than RF chains, to transmit multiple data streams via spatial multiplexing. Some selected algorithms were implemented from articles for calculating baseband and analog weights to optimize the spectral efficiency. Investigated algorithms include Yu (2018) [1], Hu (2019) [2], Yu (2017) [3], Wu (2018) [4] and Ayach (2014) [5]. The work was carried out through Monte Carlo simulations in MATLAB with a cluster based mm-wave channel model. Fully connected and partially connected RF architectures were investigated, as well as a more general group connected solution. In order to weigh performance against hardware complexity and power consumption, a literature study of mm-wave transceivers was done and a model developed for estimation of area, number of diodes and consumed DC power. At a transmit SNR of 0 dB, a spectral efficiency of 22 bps/Hz could be reached with single-user hybrid beamforming with 64 transmit antennas, 16 receive antennas, 4 parallel data streams and a fully connected transmitter. With a partially connected transmitter, the result was around 15 bps/Hz. At SNR below -25 dB, analog beamforming outperformed multi-stream transmission. Above 15 dB, the spectral efficiency of full MIMO had a slope of 4.3 bps/Hz/dB and fully connected hybrid systems reached 1.3 bps/Hz/dB. Phase shifters could be limited to 4 control bits with negligible performance loss. Overall, the Wu (2018) [4] and Hu (2019) [2] algorithms were found to be the most energy and hardware efficient.

Keywords: Hybrid beamforming, mm-wave, weight algorithms, cluster-based channel model, MIMO, spatial multiplexing

Contents

Abbreviations

bps Bits per second.

CMOS Complimentary Metal-Oxide-Semiconductor.
CSI Channel State Information.

DAC Digital-to-Analog Converter.
DC Direct Current.
DPS Double Phase Shifter.

FC Fully Connected.
FPS Fixed Phase Shifter.

LASSO Least Absolute Shinkage and Selection Operator.
LO Local Oscillator.
LOS Line of Sight.

MIMO Multiple Input, Multiple Output.
MMSE Mimimum Mean Square Error.

NLOS Non Line of Sight.
NMSE Normalized Mean Square Error.

OMP Orthogonal Matching Pursuit.

PC Partially Connected.
PS Phase Shifter.

RF Radio Frequency.

SNR Signal-to-Noise-Ratio.
SPS Single Phase Shifter.
SVD Singular Value Decomposition.

UE User Equipment.

List of Figures

List of Tables

1
Introduction

In this section, the project will be introduced, then the aim and limitations will be stated, followed by concrete goals for the project. At the end of the section, mathematical notation that will be used in the rest of the thesis is presented.

1.1 Background

For 5G mobile communication systems, high frequency mm-wave bands are being considered beyond the bands used now for mobile communication, sub-6 bands. These bands could allow high data rates for each user connected, but due to more path loss, higher gain is required which has to be achieved through beamforming. The purpose of this thesis will be to explore how beamforming should be done in a base station to get the best performance in multiple links with mobile stations, with reasonably low complexity and cost. With this purpose, hybrid beamforming will be investigated which combines analog beamforming with massive MIMO, which stands for multiple input, multiple output. In analog beamforming, beams are directed by controlling amplitude and phase of the signal to each antenna element in an array. In massive MIMO, the channel between receiver and transmitter is estimated, and weights are applied digitally to the signal sent from each transmitting antenna to enable spatial multiplexing. Then, several data streams can be sent simultaneously over the same frequencies.
Using only massive MIMO leads to a high computational load and a complex transmitter as each antenna requires a separate RF chain. Instead, one could combine it with analog beamforming to use a smaller number of RF chains. Phase shifters may be included before each antenna to give the system the ability of analog beamforming. The hybrid system combines digital precoding and the possibility to send several different signals, with analog beamforming. The result becomes less complex and may have a performance close to massive MIMO. Challenges for hybrid beamforming investigated in this thesis include which algorithm should be used to choose the weights and which antennas should connect to which RF chains.

1.2 Previous Work

Hybrid beamforming has become an increasingly hot topic over the last few years, sparked by an article by Ayach et al. (2014) [5]. They developed a method based on the orthogonal matching pursuit (OMP) algorithm, which is codebook based where the precoding matrix is taken as a linear combination of the antenna array's

response vectors. A later article by Alkhateeb et al. (2015) [6] also generalized this initial work to multi-user systems. A very high-performing algorithm based on direct optimization by gradient descent on a manifold, MO-AltMin, was presented by Yu et al [7] for single-user MIMO systems. However, the computational complexity of the algorithm was very high. The same approach was used to develop similar algorithms utilizing alternating minimization by rewriting the objective to minimize bounds instead of the effective channel directly [7]. This indirect optimization lead to lower results, but resulted in a significant speed-up. The same authors have also suggested novel hardware configurations such as fixed phase shifters with a complementary switch network [1] and pairs of fixed amplitude phase shifters in parallel, which performs well but may be difficult to realize [3].
Many articles on the subject assume fully connected systems where all RF chains connect to all antennas, which offer more degrees of freedom and allow close to optimal performance [8][1]. While this type of architecture can be argued to be unrealistic in a practical system due to hardware cost and complexity, results can be used as upper bounds for more realistic systems. Other works have explored architectures with fewer connections, such as Hu et al. (2019) [2] and Wu et al. (2018) [4] where partially connected structures are explored, meaning that each antenna connects to only one of the RF chains. Such a system leads to lower capacity, but a much simplified hardware implementation. In Yu et al. (2018) [1] it is suggested that an antenna may connect to several RF chains but not necessarily all. This architecture is a trade-off between performance and complexity.
There has been some experimental work focused on building hardware to realize hybrid beamforming, for example in Mondal (2018) [9] where a fully connected receiver with 8 antennas and 2 RF chains was constructed. There are also examples of partially connected systems capable of hybrid beamforming [10].

1.3 Aim

The aim of this project was to research hybrid beamforming solutions that can maintain a high data rate and signal-to-noise-and-interference ratio with low system complexity, power consumption and cost. As these investigations were done with simulations, an important aspect was how to set up realistic channel simulations. Choosing weights for the analog phase shifters and the digital precoding can be done in many different ways, following different algorithms. This thesis has explored a few selected algorithms that aim to maximize the spectral efficiency. In order to ensure low power consumption and low complexity, the efficiency of the used algorithms and used architectures was also investigated. An end-goal was to describe a final system that could be built and tested in a future thesis.

1.4 Limitations

The thesis was limited to researching literature, setting up beamforming scenarios and evaluating the performance through computer simulations. No physical experiments were done, but future testing was proposed.

One limitation was to focus on uniform arrays, as it allowed for a simpler search for optimal solutions. For a pratical implementation, it may be interesting to consider placing several subsystems with one RF chain and several antennas as tiles. The tile placement in that case is in itself a problem to solve, but may offer more flexibility in manufacturing.

Instead of using phase shifters for the analog part of hybrid beamforming, it is also possible to implement large switch networks or lens antennas with controllable aperture [8]. The former is likely much harder to realize at present, since fast and reliable switches are difficult to implement. This is especially true at mm-wave bands and relying on switch networks for beamforming is not feasible with current technology [8]. Lens antennas with controllable apertures have not been widely regarded so far. On this basis, this thesis was limited to phase shifters making up the analog network.

Channel estimation in hybrid beamforming is a complicated issue and it was decided to be outside the scope of this thesis. Instead, an error was added to the channel used to calculate the weights to investigate effects of having flawed channel information.

1.5 Specification of Issues Under Investigation

The end goal was to formulate a hybrid beamforming system adhering to hardware limitations, such that it can be realized in a separate, future thesis. The main areas of investigation were:

1. Which algorithm is most suitable for calculating precoding and combining weights?
2. How many antennas are suitable at the base station, and how many should be used in the user equipment?
3. How much does incomplete channel state information (CSI) affect different weight algorithms?
4. How do the different hardware configurations compare in terms of power efficiency and hardware efficiency?
5. How does phase shifter quantization affect the different algorithms?

Important considerations were how practical the chosen solutions are to build, their energy consumption and the speed of the weight calculation algorithm.

1.6 Notation

In Table 1.1, the mathematical notation used in this thesis is presented.

Table 1.1: Mathematical notation used.

Notation	Meaning
$\mathbf{A}$	Matrix
$\mathbf{a}$	Vector
$\mathbf{A}(i,j)$	Matrix element
$\mathbf{A}^T$	Transpose
$\mathbf{A}^*$	Conjugate
$\mathbf{A}^H$	Hermite conjugate (conjugate transpose)
$\text{blkdiag}(A_1, \ldots, A_n)$	Block diagonal matrix: matrices $A_1, \ldots, A_n$ on the diagonal and zeroes everywhere else
$\lvert\mathbf{A}\rvert$	Determinant of the matrix
$\lVert\mathbf{A}\rVert_F$	Frobenius norm of matrix
$\lVert\mathbf{A}\rVert_\infty$	Infinite Schatten norm of matrix
$\lVert\mathbf{A}\rVert_1$	One Schatten norm of matrix
$\lVert\mathbf{a}\rVert_2$	l_2 norm of vector
$\Re(a)$	Real part of $a \in \mathbb{C}$
$\Im(a)$	Imaginary part of $a \in \mathbb{C}$
$\angle(a)$	Angle of $a \in \mathbb{C}$
$\text{tr}(\mathbf{A})$	Trace of $\mathbf{A}$
$\text{vec}(\mathbf{A})$	Vectorization of matrix
$\mathbb{1}\{\mathbf{A} > \mathbf{B}\}$	Indicator function, returns matrix with element (i,j) equal to 1 iff $\mathbf{A}(i,j) > \mathbf{B}(i,j)$, and 0 otherwise
$\mathbf{I}_n$	Identity matrix of size $n \times n$

2

Systems for Beamforming and Simulation Theory

In this section, the need for hybrid beamforming will be discussed by exploring limitations of analog beamforming and MIMO. Then, notation will be established which will be used to describe the system throughout the report. The assumptions on hardware specifics are presented, for the purpose of comparing the different architectures. Finally, issues regarding the channel estimation will be explained.

2.1 Characteristics of mm-Wave Channels

A mm-wave band can be described as a frequency band for transmission at frequencies between 30 GHz and 300 GHz [8]. In this thesis, the focus will be on a band at 28 GHz. This is still usually regarded as a mm-wave band to distinguish it from the more conventional frequency bands exclusively used up until 4G technology, called sub-6 bands as the freqencies are lower than 6 GHz. A channel is the wireless signal path from a transmitter antenna to a receiver antenna. In the case of MIMO systems, there are as many channels as the number of input ports multiplied by the number of output ports.
One important difference between the conventional channels and the emerging mm-wave channels is the higher loss in the latter. There are two important mechanisms behind this. First, the received power P_r in a wireless link can in the simplest case be described by Friis' equation. Given some transmitted power P_t, carrier frequency f_c, speed of light c, distance r and transmitter and receiver gain G_t and G_r, the relationship is given by Equation 2.1 [11]

$$P_r = P_t G_t G_r \frac{c^2}{(4\pi r f_c)^2}. \tag{2.1}$$

Since the received power is proportional to f_c^{-2}, links operating at higher frequency experience higher loss. Secondly, the shorter wavelength leads to more scattering with the environment. For example, attenuation due to rain increases sharply above 10 GHz [12]. Together, these effects cause a much higher path loss in mm-wave channels than in sub-6 channels.
Another important consideration is how large the antenna arrays can reasonably be built for the different frequency bands. An antenna array is a set of antennas arranged close together. The signal at a far-field point is then the sum of the signals from each antenna element, but due to the separation of the elements at the

array, the summed signals have slightly different phases. This causes constructive and destructive interference. This effect is stronger for arrays with more antenna elements, causing the lobe widths to decrease as the number of antenna elements increases, and the gain in the lobe direction to increase as more of the signal is concentrated to this direction. In order to control where the signal is directed, the signal to each antenna should be possible to modify, giving the main benefit of an antenna array: a controllable main lobe without mechanical changes. A common separation of elements is $\lambda/2$ where λ is the wavelength, meaning a short wavelength allows for denser packing of antennas. Since antenna array realizations are in general limited in size, a higher frequency allows for more antenna elements, which gives a higher gain in the main lobe direction. By this, mm-wave channels may compensate for their path loss by using more antennas.
As mentioned, the wave is more prone to scattering instead of reflecting due to the high frequency. This can be understood by noting that for objects of roughly the same size as the wavelength or larger, radiation interacts via scattering instead of reflections [13]. At 28 GHz, the wavelength in air is approximately 1 cm, while at for example 6 GHz, the wavelength in air is 5 cm. This means that sub-6 signals are much less disturbed by small objects in the channel, while mm-wave signals have stronger interactions with for example leaves. The result of the increased scattering is that while the signal can take several paths from the transmitter, it is unlikely that many reach the receiver and are sampled in the same time slot. This is referred to as having a sparse channel [14]. Rich channels with many contributions at once are more common at lower frequencies or in indoor environments. Having a sparse channel is relevant to how the channel is estimated in a transmission scheme, which will be touched upon in Section 2.7.

2.2 Analog and fully digital beamforming

While using a large number of antennas in the array can be beneficial for the communication link, it can be difficult to construct depending on the implementation. In fully digital MIMO antenna arrays, a unique signal is passed to each antenna by connecting one RF chain per antenna. An example of a typical transmitter RF chain is presented in Figure 2.1. The first step, 1, is a digital-to-analog converter (DAC) which converts some digitally pre-processed signal to a low-frequency, baseband signal, f_{IF}. Step 2 depicts a pre-amplifier which amplifies the signal, adding as little noise as possible. In step 3, the signal is passed into an upconverting mixer. It also takes input from a local oscillator (LO) which provides a signal with frequency f_{LO}. The output from the mixer is ideally a signal with frequency components $f_{\text{LO}} + f_{\text{IF}}$ and $f_{\text{LO}} - f_{\text{IF}}$. Therefore, in step 4, a filter is applied to isolate one component. Let $f_{\text{RF}} = f_{\text{LO}} + f_{\text{IF}}$ be the signal that passes through. For a large difference between f_{IF} and f_{RF}, it may be necessary to use several mixers and LO to upconvert the signal in steps, since filters cannot be made arbitrarily narrow. After the upconversion, a power amplifier (step 5) is used, which may have a larger noise figure than the pre-amplifier, but provides a higher power output.
MIMO is a developing technology where several data streams are transmitted at once. With several connected RF chains, the signal to each antenna is weighed

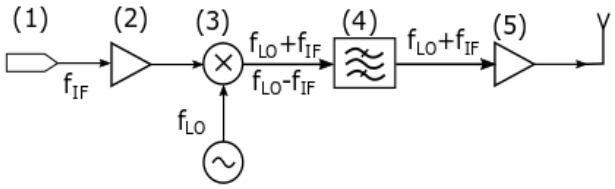

Figure 2.1: Example of an RF chain at a transmitter, complete with DAC (1), preamplifier (2), upconvering mixer with local oscillator (3), bandpass filter (4) and a power amplifier (5). The arrows indicate signal path.

in order to transmit several data streams at once and at the same frequency to different locations. This is called spatial multiplexing and relies on beams being narrow enough to avoid mixing signals intended for different users. Channel sparsity is another important aspect, because the signals could also overlap if there are too many reflections on the way, allowing the signals to mix together. Ideally, the transmitted signals have independent channels.

The center frequency assumed in this work is $f_{\mathrm{RF}} = 28\,\mathrm{GHz}$. Selected specifications for components working at this frequency are presented in Table 2.1. As can be seen from the data, constructing an individual RF-chain for each antenna in a large array would be complicated, expensive and consume a lot of power. Additionally, the equivalent channel at baseband can be represented by a matrix with size given by the number of RF chains. Determining weights for the transmission typically involves inversion and single-value decomposition of the equivalent channel, which becomes very computationally complex for large matrices.

For the single user, single stream case, a phased array based on analog beamforming can be done. This only requires a single RF chain and then modifies the signal passed to each antenna in the analog domain. A phase shifter connected before each antenna is used to manipulate the phase of the signal sent to each antenna, in order to steer the lobe direction.

The phase shifter can be implemented in different ways, where one example is by switching to and from delay lines. As the signal travels a longer path, the phase is changed. As the electrical length is a linear function of the frequency given the physical length, the phase at the output is a linear function of frequency. Another variant can be made using a combination of low and high pass filters. The response using this method is less frequency dependent [15]. Variable phase shifters can not take on arbitrary phases, but are rather designed to take on a set of discrete values. They can be realized by connecting a series of phase shifting elements of set values who are then switched in or out, so the phase can be represented as a binary number. Typically, phase shifters have 5 or 6 control bits. resulting in 32 or 64 avaliable values spread over angles in $[0,2\pi)$. This results in limitations on the analog beamforming, as the angular resolution is lacking and the update frequency of the phase shifters can limit the time to move the beam. Additionally, since only one RF chain is employed, the system can only communicate with a single user at a given frequency and time slot. A big advantage of MIMO is that the multiple streams allows for spatial multiplexing, but this cannot be done with analog beamforming.

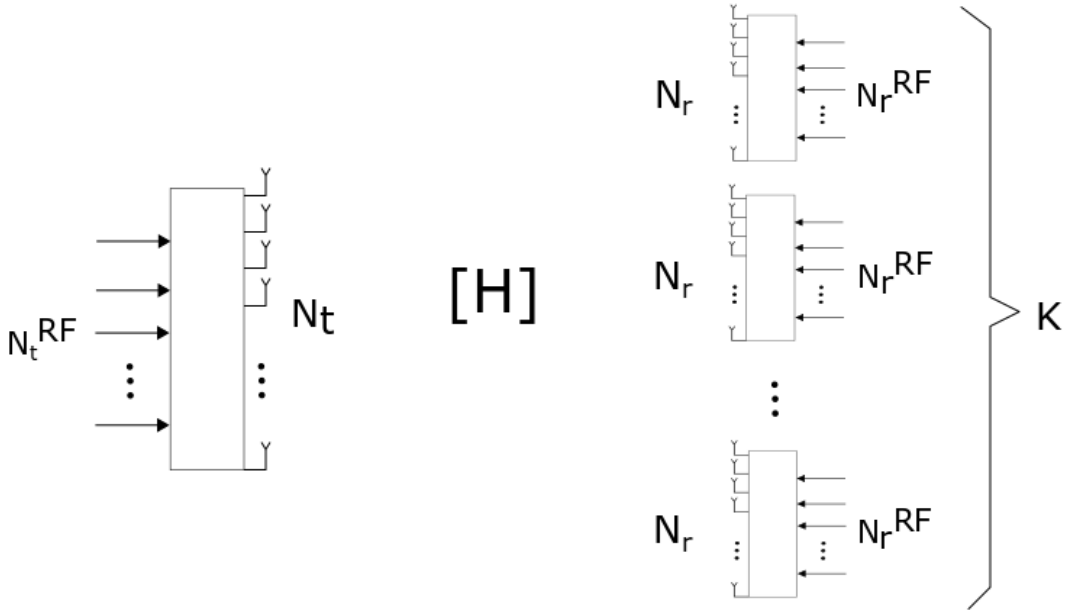

Figure 2.2: Illustration of number of RF chains and number of antennas at transmitter and receiver, respectively. The channel matrix $\mathbf{H}_{i,j}$ maps the signal from transmitter antenna j to receiver antenna i.

2.3 Hybrid Beamforming

A natural extension to analog beamforming is increasing the number of RF chains and thereby allowing transmission of several data streams at once, while still keeping the phase shifters and using fewer RF-chains than antennas. This is called hybrid beamforming, where digital precoding over the available RF chains is done to weigh signals to get spacial multiplexing, and then adding a layer of analog beamforming to control the signal to each specific antenna. The basis for description of the system is found in Figure 2.2, with N_t base station antennas, N_r antennas per user equipment (UE), N_t^{RF} RF chains at the base station and N_r^{RF} chains at the UE. A total of K users are present and each user receives N_s data streams.

An important characteristic of a system using hybrid beamforming is how the antennas are connected to the RF chains. A proposed version common in the literature is the fully connected (FC) architecture, where all RF chains connect to all antennas, as in Figure 2.3a. In an FC system, in total $N_t N_t^{\mathrm{RF}}$ phase shifters are used. This offers a large degree of freedom in designing the weights, but the number of phase shifters becomes large which causes high power consumption and high system complexity. The cost per phase shifter may be high, especially if high resolution is desired. Another issue in realizing the fully connected system is the signal crossover. If the circuit is built on a chip, it may potentially cause insurmountable issues in design, and signal leakage may degrade the functionality. Instead, one can connect

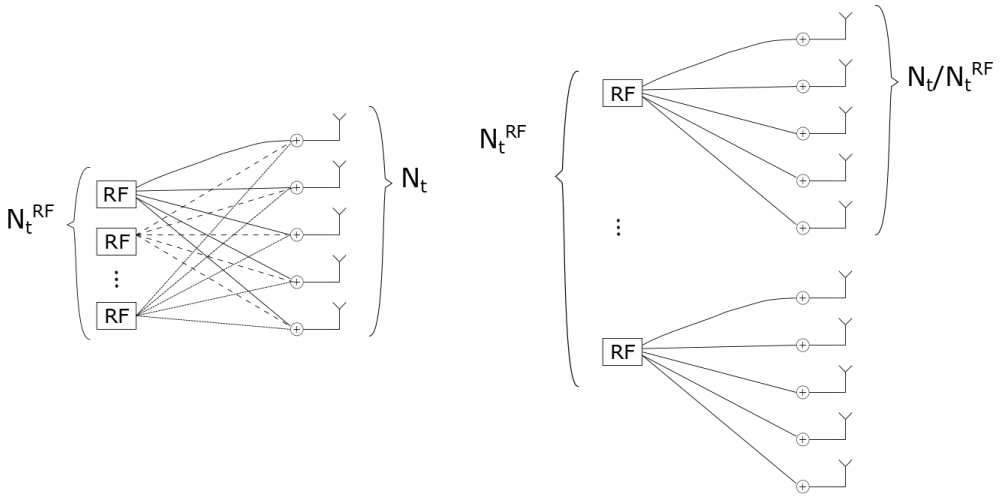

(a) Fully connected (FC) ***(b)*** Partially connected (PC)

Figure 2.3: Illustration of the fully and partially connected architectures. In the FC case, all antennas chains are connected to all RF chains, while in the PC case, each antenna connects to only one RF chain.

each antenna to only one RF chain, but several antennas to each RF chain. This is often called a partially connected (PC) or sub-connected system and is illustrated in Figure 2.3b. Now, only N_t phase shifters are needed and crossovers can be avoided. The drawback is degraded performance.
A more general way of constructing the mapping is by using a group connected architecture as proposed in [1]. Another article that proposes a similar mapping is [16], where it is called a hybrid connection. Instead of only considering the extreme cases of connecting all RF chains to all antennas, or each antenna to only one RF chain, this architecture allows for one antenna to connect to any number of RF chains. More specifically, the RF chains and antennas are divided into η groups, then all RF chains are connected to all antennas within each group. An example is illustrated in Figure 2.4, where the lines represent connections that in a real system would also include a phase shifter. This also covers the previously discussed architectures, as the fully connected structure is achieved by setting $\eta = 1$, and the partially connected by setting $\eta = N_t^{\mathrm{RF}}$.
How the UE is constructed can vary a lot in the literature. Typically, the UE is assumed to be much simpler than the base station, with much less available power and fewer antennas due to space and battery limitations. In this work, 16 or fewer antennas per user will be assumed unless otherwise stated. The UE is assumed to perform hybrid beamforming with at most four RF chains. Then, each user can only handle at most four data streams.

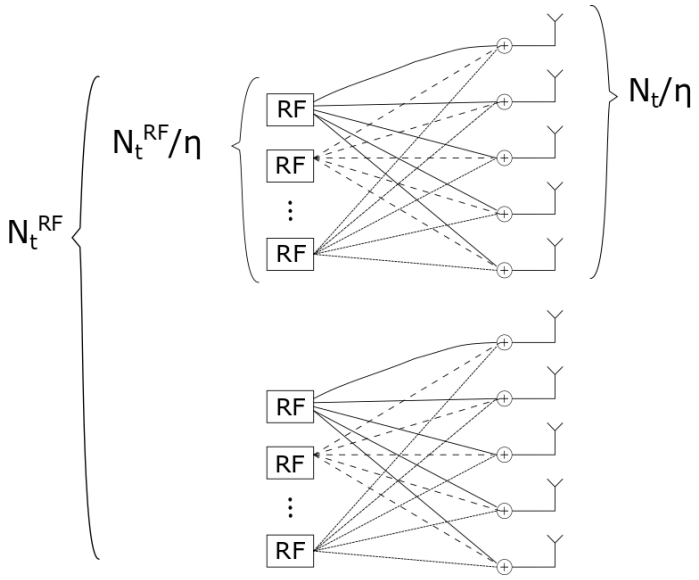

Figure 2.4: Illustration of a group connected architecture. The N_t^{RF} RF chains and N_t antennas are divided into η groups. Within the groups, the systems are fully connected.

2.4 The Fixed Phase Shifter (FPS) Implementation

An novel approach to increase the degrees of freedom of the analog network was taken in Yu (2018) [1], where the use of a multi-channel and non-adjustable phase shifter is proposed [17]. For each signal path, a switch is used to pass or block the signal and the signals are combined afterwards. This is different from the phase shifters discussed in Section 2.2 where the phase shifters can be decomposed to serially connected phase shifters of fixed phases, with switches to include or exclude one phase shifter's contribution. In [1], the phase shifters are instead connected in parallel. The total signal for a series connection y_s and a parallel connection y_p respectively become:

$$y_s = \sum_{i=1}^{N_c} s_i p_i, \qquad y_p = \frac{1}{\sum_{i=1}^{N_c} \frac{s_i}{p_i}}, \tag{2.2}$$

where p_i is the phase of phase shifter i and s_i can take on values 0 and 1, and indicates whether the switch is on or off. As a result, the approach by Yu [1] is fundamentally different and cannot be correctly represented by regular phase shifters. However, the article about multi-channel phase shifters [17] refers to phase shifters with separate channels for different frequencies, while the FPS implementation would require a phase shifter with multiple channels for one frequency. Therefore, this thesis will simulate an FPS implementation with multiple sets of fixed phase shifters, one for each connection. This is due to the lack of a known realistic multi-channel component, but will incur a higher complexity for the FPS architectures than intended in [1].

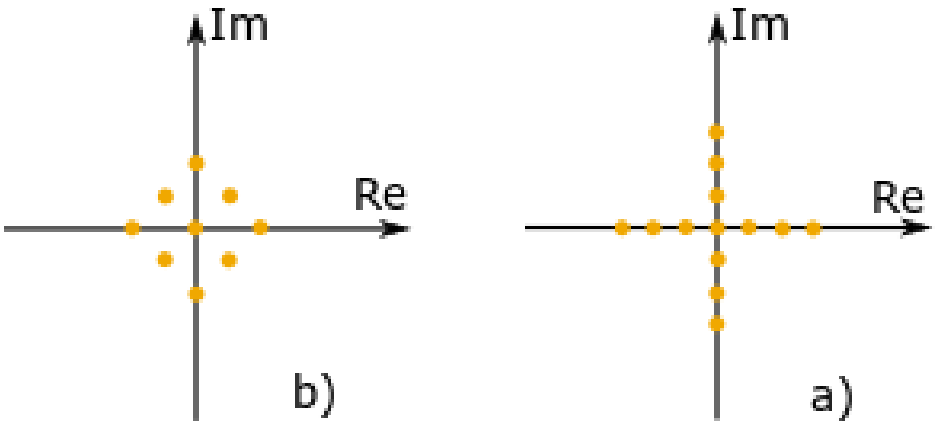

(a) DPS *(b)* PS with amplitude control

Figure 2.5: Reachable complex weight values for a quantized phase shifter. In a), two phase shifters connected in parallel are used, both with 2 bits for phase control. In b), one phase shifter with 2 bits for phase control and 2 bits for amplitude control is shown.

2.5 The Double Phase Shifter (DPS) implementation

By replacing each phase shifter in the standard Single Phase Shifter (SPS) structure with two parallel connected phase shifters, amplitude control is gained since two signals with unit amplitude but different phases are added. This was proposed in [3] as a way to increase the control over the analog weights while still using simple phase shifters. Likely, using phase shifters with built in amplitude control is more viable to implement than using twice as many phase shifters than needed. Hence, this report has focused on using the developed algorithm but with a single amplitude controlled phase shifter. In the case of infinitely precise phase shifters, these two approaches are equivalent, but the original proposal with two fixed amplitude phase shifters (PS) in [3] offer other reachable complex weight values in the quantized case. For a quantized PS with 2 bits for phase control and 2 bits for amplitude control, Figure 2.5b presents a sketch of the reachable complex values. For a parallel connection of two 2-bit fixed amplitude phase shifters, the equivalent sketch is given in Figure 2.5a.

2.6 Hardware Details

In order to compare base station architectures in terms of hardware complexity, cost and power consumption, a framework was set up detailing all of the hypothetically included components. Three different aspects were considered: DC power consumption, chip area and the equivalent number of diodes. The systems are here viewed as the sum of a set of components. For the different architectures and algorithms, the total complexity for each is calculated as in Equation 2.3. The total number of RF chain to antenna connections is denoted $\zeta = N_t N_t^{\mathrm{RF}}/\eta$, where η is the number

of groups as detailed in Section 2.3.

$$X_{\text{tot}} = N_t^{\text{RF}} X_{\text{RF}} + \zeta(X_{\text{PS}} + X_{\text{Combiner}}) + N_t X_{\text{PA}}, \tag{2.3}$$

where X represents area, DC power or number of diodes depending on which property is considered. RF stands for RF chain, PS stands for phase shifter, combiner represents the complexity per stream to combine signals before the antenna, and PA represents the power amplifier needed before each antenna. For uplink transmission, the PA would be swapped for a low noise amplifier at the antenna. In Table 2.1, the used data is presented. The value of the total area, number of diodes or power consumption was then used to calculate the efficiency of the system, as defined in Equation 2.4.

$$E = \frac{R}{X_{\text{tot}}}, \tag{2.4}$$

where R is the spectral efficiency and X_{tot} is defined in Equation 2.3.

Table 2.1: Values of DC power consumption, component chip area and the equivalent number of diodes listed for each of the used components. Values are summed for hardware comparisons.

Property	4-bit PS [18]	PS (ampl. control) [19]	Mixer [20]	LNA [20]	LO [20]	PA [21]	Switch (DT) [22]	2x2 combiner [9]
DC Power [mW]	0	27	0	38.4	174	291	0	10
Area [mm^2]	0.067	0.063	0.37	0.13	0.81	0.59	0.01	0.28
Num. diodes	20	25	16	8	4	8	24	2
Technology	65-nm LP CMOS	120-nm CMOS	65-nm CMOS	65-nm CMOS	65-nm CMOS	28-nm CMOS	65-nm CMOS	65-nm CMOS
Gain [dB]	-14.1	-5	-6	10	-	22	-1.1	-
Phase error [°]	< 9.4	< 1.5	-	-	-	-	-	-
Bandwidth [GHz]	0.85	2.85	4	4	4	2.975	14.5	-

2.7 The Channel Estimation Problem

To relate the signal sent from one antenna at the BS to one antenna at the UE, a channel matrix is constructed, denoted as $\mathbf{H}$. Especially for a mm-wave channel, the elements are very sensitive to changes in the environment, since the wavelength is in the order of centimeters. To decode the received signal, the channel must be known to some extent to nullify its effect. In a real-life system, obtaining this channel information is complicated and the subject of a lot of research [8]. A common approach is sending known waveforms, pilot signals, and recording the received waveforms. However, approaches developed for MIMO systems may be hard to reuse for hybrid systems, since the number of RF chains is less than the number of antennas. Thus, the signal recorded by each antenna is not known, only a weighed sum from all antennas connected to one RF chain is available. The problem is said to be dimension deficient. Because of this, there is not yet an optimal method for channel estimation for hybrid beamforming systems and due to the complexity of the problem, no channel estimation has been implemented in this work. In most cases in this work, the channel matrix was assumed to be known at both receiver and transmitter.

2.8 Spectral efficiency

Spectral efficiency describes the information rate over the transmission bandwidth. For a single antenna transmitter and single antenna receiver, the maximum spectral efficiency is given by Shannon's channel capacity theorem [23]

$$\frac{C}{B} = \log_2(1 + \mathrm{SNR}), \tag{2.5}$$

where C is the capacity in bits/s, B is the bandwidth in Hz and SNR stands for signal-to-noise-ratio. Here, it is referred to the receiver. In this work, the SNR is defined as:

$$\mathrm{SNR} = \frac{P_t}{N_0}, \tag{2.6}$$

where P_t is the total transmitted power before the transmit antenna array and N_0 is the noise power at the receiver. To find the capacity, the SNR at the receiver should be used, which uses the received power.
With this definition, the spectral efficiency R achieved for some combining weights $\mathbf{W}$, channel $\mathbf{H}$ and precoding weights $\mathbf{F}$ and in total N_s transmitted data streams in parallel to one user can be written as [5]

$$\mathbf{H}_{\mathrm{eq}} = \mathbf{W}^H\mathbf{H}\mathbf{F}, \tag{2.7}$$

$$R = \log_2\left(\left|\mathbf{I}_{N_s} + \frac{\mathrm{SNR}}{N_s}(\mathbf{W}^H\mathbf{W})^{-1}\mathbf{H}_{\mathrm{eq}}\mathbf{H}_{\mathrm{eq}}^H\right|\right), \tag{2.8}$$

where SNR is the signal-to-noise-ratio as defined in Equation 2.6 and $\mathbf{H}_{\mathrm{eq}}$ is the baseband-to-baseband channel matrix.

3

Channel Simulation and Evaluation Tools

Initially, the posed questions were investigated through literature studies. Many investigations have been done on hybrid beamforming systems, but most are done with simulations, so comparisons with real implemented systems are scarce. In this work, Monte Carlo simulations are used and in this chapter, the simulation procedures are described. This includes how the channels were simulated and how the performance was estimated, and while the work described in this chapter is not the focus of the thesis, it should be considered the foundation for the investigated beamforming algorithms.

3.1 Definition of Channel Matrix

In the literature, the received and decoded $\mathbb{C}^{N_s \times 1}$ signal $\mathbf{y}$ is commonly defined as:

$$y = \mathbf{W}^H \mathbf{H} \mathbf{F} x + \mathbf{W}^H n, \tag{3.1}$$

where $\mathbf{W}$ is the $\mathbb{C}^{N_r \times N_s}$ combining matrix, $\mathbf{H}$ is the $\mathbb{C}^{N_r \times N_t}$ channel matrix, $\mathbf{F}$ is the $\mathbb{C}^{N_t \times N_s}$ precoding matrix, $\mathbf{x}$ the $\mathbb{C}^{N_s \times 1}$ transmitted signal and n is $\mathbb{C}^{N_r \times 1}$ additive noise. In some instances, predefined MATLAB methods have been used. A notable thing is that MATLAB defines the received signal and the channel matrix as:

$$\tilde{\mathbf{y}} = \tilde{\mathbf{x}} \tilde{\mathbf{F}} \tilde{\mathbf{H}} \tilde{\mathbf{W}} + \mathbf{n} \tilde{\mathbf{W}}. \tag{3.2}$$

With this definition, $\tilde{\mathbf{x}}$ and $\tilde{\mathbf{y}}$ are $\mathbb{C}^{1 \times N_s}$ vectors, $\tilde{\mathbf{F}}$ is $\mathbb{C}^{Ns \times N_t}$, $\tilde{\mathbf{H}}$ is $\mathbb{C}^{N_t \times N_r}$ and $\tilde{\mathbf{W}}$ is $\mathbb{C}^{N_r \times N_s}$. Since the elements of $\tilde{\mathbf{x}}$ and $\tilde{\mathbf{y}}$ should be the same as in $\mathbf{x}$ and $\mathbf{y}$, taking the transpose of Equation 3.2 should equal Equation 3.1, noting that $(AB)^T = B^T A^T$. Consequently, one can move between the definitions by using $\tilde{\mathbf{F}} = \mathbf{F}^T$, $\tilde{\mathbf{W}} = \mathbf{W}^*$ and $\tilde{\mathbf{H}} = \mathbf{H}^T$.
In the case of multi-user transmission, a channel $\mathbf{H}_k$ is generated between the base station and user k. The total channel matrix for all K users is then given by:

$$\mathbf{H} = [\mathbf{H}_1^T, \ldots, \mathbf{H}_K^T]^T. \tag{3.3}$$

If the user k combining matrix is written as $\mathbf{W}_k \in \mathbb{C}^{N_r \times N_r^{\mathrm{RF}}}$, the combiner matrix containing all users can be written as blkdiag$(\mathbf{W}_1, \ldots \mathbf{W}_K)$. At the transmitter, the digital precoding matrix $\mathbf{F}_{\mathrm{BB},k}$ is different for transmission to each user and is of

size $\mathbb{C}^{N_s \times N_s}$, so that the common matrix $\mathbf{F}_{\text{BB}} = [\mathbf{F}_{\text{BB},1}, \ldots, \mathbf{F}_{\text{BB},K}] \in \mathbb{C}^{N_s \times KN_s}$. The analog precoding matrix is shared for all users.
In order to have comparable results, the channel matrix must be normalized such that the expected value of the square Frobenius norm equals the number of elements, i.e. $\mathbb{E}[\|\mathbf{H}\|_F^2] = N_r N_t$ [5]. This makes it possible to compare results derived using different channel models, and to modify the elements and renormalize them, for example to add an error or to amplify one path gain to simulate line-of-sight (LOS) conditions.
In order to investigate the effect of channel estimation errors, a random error was added for each element of the channel matrix. The resulting channel matrix, $\mathbf{H}_{\text{est}}$, was used to calculate the beamforming weights, while the original matrix, $\mathbf{H}$, was used to evaluate the channel capacity. Call the random variable containing the errors X, then let each element in X be i.i.d. $x_{i,j} \sim \mathcal{CN}(0,1)$. Then, form the channel estimate that includes an error by

$$\mathbf{H}_{\text{est}} = \frac{\mathbf{H} + \sqrt{e}X}{\sqrt{1+e}}, \tag{3.4}$$

where e is the error variance which here was kept in the range $0 \leq e \leq 5$. Then, the normalized mean square error (NMSE) was estimated for the different error variances. In total, M different channel instances were simulated, so letting $\mathbf{H}^m$ and $\mathbf{H}_{\text{est}}^m$ be the m:th simulated channel and estimated channel, the NMSE was calculated as

$$\text{NMSE} = \frac{\sum_{m=1}^{M}\sum_{i=1}^{N_r}\sum_{j=1}^{N_t}|\mathbf{H}^m(i,j) - \mathbf{H}_{\text{est}}^m(i,j)|^2}{\sum_{m=1}^{M}\sum_{i=1}^{N_r}\sum_{j=1}^{N_t}|\mathbf{H}^m(i,j)|^2}. \tag{3.5}$$

3.2 Cluster Based Channel Model

The channel model mostly used in this thesis is a clustered channel model based on the extended Saleh-Valenzuela model, as outlined in Ayach et al. (2014) [5]. It was implemented based on an example from Mathworks on hybrid beamforming [24]. The channel is simulated by assuming N_{cl} scattering clusters, each giving rise to N_{ray} rays, which is visualized in Figure 3.1. The clusters are placed at random angles from the receiver and the transmitter, and a random contribution is added to the angle of incidence for each ray. In addition, each ray is assigned a complex propagation constant, corresponding to both attenuation of the path as well as phase shift. The cluster angles were generated from uniform distributions, with the added angle for each ray taken from a normal distribution. The gain was generated from a standard complex normal distribution. The choice of N_{cl} and N_{ray} would depend on the simulated environment. These numbers should be kept low, since the channel is sparse as noted in Section 2.1. However, it was found from the simulations that the total number of scatters, $N_{\text{cl}}N_{\text{ray}}$, should be at least equal to the smallest dimension of the channel matrix, N_r to avoid rank deficiency. Additionally, there should be at least as many clusters as there are data streams in order to allow spatial multiplexing.

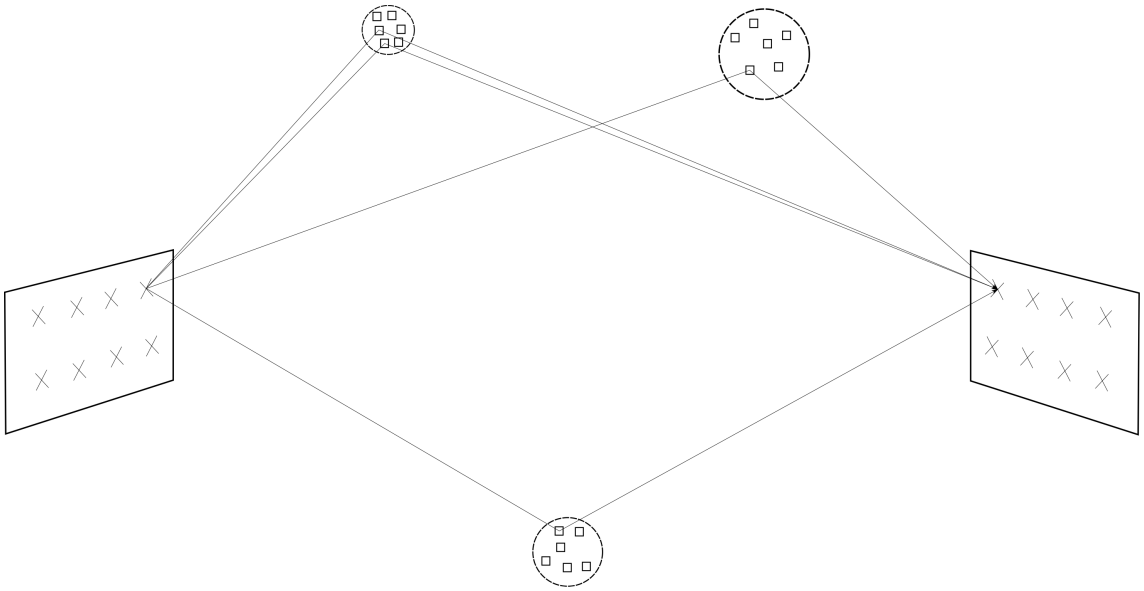

Figure 3.1: Visualization of cluster based channel model. Here, transmitter and receiver antenna arrays had 8 antenna elements each. Three clusters are drawn, each containing 6 scatterers. Four out of the 18 multipaths are drawn as lines. The channel matrix element is given as a sum over all multipaths.

To simulate the antenna array responses, `PartitionedArray` objects were generated from the Phased Array System toolbox in MATLAB. With these objects and the randomly selected cluster positions and gains, the function `scatteringchmtx` was used to generate a channel matrix $\mathbf{H}$. As noted in Section 3.1, the used channel was then found by transposing the result.
To simulate LOS conditions, the amplitude of the gain was amplified by a factor of 100 for all rays related to the first cluster. The gain was then normalized such that the channel fulfilled its expected Frobenius norm.
In the case of broadband transmission with multiple subcarriers, the same angles and gains for the rays were used for all subcarriers. While the angles would be the same, the gain may not be this flat in reality, as some variations in response are expected when the frequency varies. An appropriate gain variation over the bandwidth would need more investigation. The channel matrices were still different due to the different array responses. The array elements had a physical spacing of $0.5\lambda_c$ where λ_c was the wavelength at the center frequency. The perceived spacing was then different over the bandwidth.

3.3 NYUSIM Channel Model

Another approach to simulate the channel matrix was to use a premade model. One such example is the NYUSIM 5G channel model made based on extensive measurements [25]. An open-source channel simulator is provided, which allows for time-coherent or drop based simulations with a randomized distance between the UE and the base station. For the Monte Carlo simulations done in this work, the

drop-based mode was utilized which simulates a number of independent positions around the base station and returns the angles of acceptance and departure, the path loss, time delay and phases. Both the LOS and the NLOS cases could be simulated using this. Here, only the UMi scenario was considered, which stands for urban microcell. This would be a cell used to cover small, densely populated areas in cities, with a range of below 500 m [25]. In order to compare the results with the clustered channel model, the calculated channel elements were normalized such that $\|\mathbf{H}\|_F^2 = N_r N_t$.

3.4 Performance Calculation

The performance metric used was the spectral efficiency, described in Section 2.8. For the single user case, the spectral efficiency was calculated as in Equation 2.7 with $\mathbf{W} = \mathbf{W}_{\mathrm{RF}}\mathbf{W}_{\mathrm{B}}$ and $\mathbf{F} = \mathbf{F}_{\mathrm{RF}}\mathbf{F}_{\mathrm{B}}$.
In the multiple user case, following [2], the sum rate, or total spectral efficiency for all users, was calculated as

$$R_{\mathrm{sum}} = \sum_{k=1}^{K} \log_2 \left| \mathbf{I} + \frac{P}{KN_s}\mathbf{R}_k^{-1}\mathbf{W}_{k,\mathrm{B}}^H\mathbf{W}_{k,\mathrm{RF}}^H\mathbf{H}_k\mathbf{F}_{\mathrm{RF}}\mathbf{F}_{k.\mathrm{B}}\mathbf{F}_{k,\mathrm{B}}^H\mathbf{F}_{RF}^H \mathbf{H}_k^H\mathbf{W}_{k,\mathrm{RF}}\mathbf{W}_{k,\mathrm{B}} \right|, \tag{3.6}$$

$$\mathbf{R}_k = \frac{P}{KN_s}\sum_{i\neq k}\mathbf{W}_{k,\mathrm{B}}^H\mathbf{W}_{k,\mathrm{RF}}^H\mathbf{H}_k\mathbf{F}_{\mathrm{RF}}\mathbf{F}_{i.\mathrm{B}}\mathbf{F}_{i,\mathrm{B}}^H\mathbf{F}_{\mathrm{RF}}^H\mathbf{H}_k^H\mathbf{W}_{k,\mathrm{RF}}\mathbf{W}_{k,\mathrm{B}} + \\ + \sigma^2\mathbf{W}_{k,\mathrm{B}}^H\mathbf{W}_{k,\mathrm{RF}}^H\mathbf{W}_{k,\mathrm{RF}}\mathbf{W}_{k,\mathrm{B}}, \tag{3.7}$$

where σ^2 is the noise variance and P the signal power. As noted in Section 3.1, matrices with subsript k denote the channel or weights for user k, for the in total K users. The matrix $\mathbf{R}_k$ contains the interference and noise for user k. In the case of multiple subcarriers, the calculation was repeated for each one, summed and divided over the total number of subcarriers, as the spectral efficiency is expressed as maximum rate over frequency.
To investigate the effect of phase shifter quantization, a set of allowed values were set up. For phase quantization, 2^{d_p} values evenly distributed in [0,2π) were chosen, where d_p is the number of bits. Equivalentely, for amplitude quantization, the maximum value, max($|\mathbf{A}|$), was set as the maximum value of the matrix to quantize, then 2^{d_a} values were set up in range [0,max($|\mathbf{A}|$)], where d_a was the number of bits for setting the amplitude. For each element in the analog matrices, the closest allowed value was chosen.

4

Weight Determination Algorithms

This chapter aims to describe the different algorithms used for calculating the weights applied to the signals for pre- and decoding. Alongside Chapter 3, it describes how the simulations were performed.
A number of different algorithms were tested to calculate the weights in baseband pre- and decoding matrices $\mathbf{F}_{\mathrm{B}}$ and $\mathbf{W}_{\mathrm{B}}$, as well as in the analog, RF precoding matrices $\mathbf{F}_{\mathrm{RF}}$ and $\mathbf{W}_{\mathrm{RF}}$. In order to compare them, the resulting sum rates of the systems were calculated as in Equation 3.6 for different values of transmit SNR. The same expression holds for single-user systems where $K = 1$. A general way to describe the mapping of RF chains to antennas is with the group connected model as seen in Figure 2.4, where setting the number of groups η to 1 corresponds to a fully connected system, and setting it to N_t^{RF} answers to a partially connected system. Therefore, the algorithms are described in this section for a group-mapping scenario to cover all architectures. The goal of each algorithm is to take the channel matrix and return precoding and combining matrices which give the optimal sum rate.

4.1 Optimal Weights

A limitation of finding the hybrid beamforming weights is that they are given as the product of two matrices. The optimal weights are given as the unconstrained precoding weights, not taking the specifics of the hybrid construction into account. The dimension of the optimal weights is therefore $N_t \times N_s$ on the transmitter side, and $N_r \times N_s$ on the receiver side. The used weights were based on an example given by Mathworks on hybrid beamforming [24]. For the single-user case, the optimal precoding weights were given by taking the singular value decomposition of the channel matrix. The N_s first right-singular vectors could then be taken directly to form the precoding weights. To form the combining matrix, a mimimum mean square error (MMSE) estimator was used. The optimal decoding weights can be written as [5]

$$\mathbf{W}_{\mathrm{opt}} = \left[\left(\mathbf{F}_{\mathrm{opt}}^H \mathbf{H}^H \mathbf{H} \mathbf{F}_{\mathrm{opt}} + \frac{N_s}{\mathrm{SNR}} \mathbf{I}_{N_s} \right)^{-1} \mathbf{F}_{\mathrm{opt}}^H \mathbf{H}^H \right]^H . \tag{4.1}$$

In the multi-user case, an algorithm that forces block diagonality of $\mathbf{W}^H\mathbf{H}\mathbf{F}$ is used [26]. Let $\mathbf{W}$ be block diagonal itself and determine each block as for the single-user case, by taking the first left eigenvectors of the channel. The challenge is now to design the precoder such that the block diagonality holds. With the combiner

decided, define a matrix $\mathbf{H}_{\text{eq}} = \mathbf{W}_{\text{opt}}^H \mathbf{H}$ as the new equivalent channel and $\bar{\mathbf{H}}_k$ which excludes user k, as

$$\bar{\mathbf{H}}_k = [\mathbf{H}_{\text{eq},1}^T, \ldots, \mathbf{H}_{\text{eq},k-1}^T, \mathbf{H}_{\text{eq},k+1}^T, \ldots, \mathbf{H}_{\text{eq},K}^T]^T \tag{4.2}$$

In order to cancel out interference from the other users, the subset of digital transmitter weights $\mathbf{F}_{\text{B},k}$ should lie in the nullspace of $\bar{\mathbf{H}}_k$. This can be extracted by taking the singular value decomposition of $\bar{\mathbf{H}}_k$. Let $\bar{L}_k$ be the rank of $\bar{\mathbf{H}}_k$. The right nullspace is then the last $N_t - \bar{L}_k$ right eigenvectors, called $\bar{\mathbf{V}}_k^{(0)}$ Now, we can form another equivalent channel that has no interference between users, $\tilde{\mathbf{H}}_k = \mathbf{H}_k \bar{\mathbf{V}}_k^{(0)}$. In order to maximize the system capacity, take the single value decomposition (SVD) of the interference-free channel matrix. Let $\tilde{L}_k$ be the rank of $\tilde{\mathbf{H}}_k$, then pick out the first $\tilde{L}_k$ right eigenvectors and denote this matrix as $\mathbf{V}_{\mathbf{k}}^{(\mathbf{1})}$. Finally, the optimal precoder can be determined as:

$$\mathbf{F}_{\text{opt}} = [\tilde{\mathbf{V}}_1^{(0)} \mathbf{V}_1^{(1)}, \ldots, \tilde{\mathbf{V}}_K^{(0)} \mathbf{V}_K^{(1)}] \sqrt{\mathbf{\Lambda}} \tag{4.3}$$

where $\sqrt{\mathbf{\Lambda}}$ is a diagonal matrix whose elements scale the power transmitted to each user. These elements are found by utilizing the `waterfill` MATLAB function. The purpose is to distribute the signal depending on the noise in each equivalent channel. This can be useful if the communication between one pair of RF chains is very poor, letting the signal be send via the other pairs instead, since the receiever in the end is one and the same.

4.2 Hu (2019) Algorithm

This method was proposed in [2] for fully connected and partially connected architectures. In this work, it has been extended to cover general group connected architectures. The used phase shifters are assumed to be without amplitude control. They start by designing the analog beamforming weights to maximize the beamforming gain given a channel matrix. The objective is then written as:

$$\max_{\mathbf{W}_{\text{RF}}, \mathbf{F}_{\text{RF}}} |\mathbf{W}_{\text{RF}}^H \mathbf{H} \mathbf{F}_{\text{RF}}|. \tag{4.4}$$

Each non-zero element in $\mathbf{F}_{\text{RF}}$ and $\mathbf{W}_{\text{RF}}$ is constrained to fulfill $|\mathbf{F}_{\text{RF}}(i,j)| = 1/\sqrt{N_t}$, and $|\mathbf{W}_{\text{RF}}(i,j)| = 1/\sqrt{N_r}$ respectively due to lack of amplitude control.
The column iterative algorithm as in [27] was used to find the weights. The matrix optimization is decomposed into multiple vector optimization problems by rewriting the objective function as follows, where $\mathbf{w}_{\text{RF},l}$ is the l:th column vector of $\mathbf{W}_{\text{RF}}$ and $\bar{\mathbf{W}}_{\text{RF},l}$ is the remainder of $\mathbf{W}_{\text{RF}}$ after removing column $\mathbf{w}_{\text{RF},l}$.

$$|\mathbf{W}_{\text{RF}}^H \mathbf{H} \mathbf{F}_{\text{RF}}| = |\bar{\mathbf{W}}_{\text{RF},l}^H \mathbf{H} \bar{\mathbf{F}}_{\text{RF},l}| \cdot |\mathbf{w}_{\text{RF},l}^H \mathbf{G}_l \mathbf{f}_{\text{RF},l}|, \tag{4.5}$$

The variables $\mathbf{f}_{\text{RF},l}$ and $\bar{\mathbf{F}}_{\text{RF},l}$ are defined correspondingly. The matrix $\mathbf{G}_l$ is defined as $\mathbf{G}_l = \mathbf{H} - \mathbf{H}\bar{\mathbf{F}}_{\text{RF},l}(\bar{\mathbf{W}}_{\text{RF},l}^H \mathbf{H} \bar{\mathbf{F}}_{\text{RF},l})^{-1} \bar{\mathbf{W}}_{\text{RF},l}^H \mathbf{H}$. By separating the objective in this way, the weights in the l:th RF chain can be found through optimization of $|\mathbf{w}_{\text{RF},l}^H \mathbf{G}_l \mathbf{f}_{\text{RF},l}|$, as its contribution has been taken out from the total beamforming gain. The new goal is therefore $\max_{\mathbf{w}_{\text{RF},l} \mathbf{f}_{\text{RF},l}} |\mathbf{w}_{\text{RF},l}^H \mathbf{G}_l \mathbf{f}_{\text{RF},l}|$.

Now, the vector $\mathbf{f}_{\mathrm{RF},l}$ is first updated element by element by separating out the current n:th element, $\mathbf{f}_{\mathrm{RF},l}(n)$. Since G_l and $\mathbf{w}_{\mathrm{RF},l}$ are independent of $\mathbf{f}_{\mathrm{RF},l}$, the expression can be rewritten, letting $\bar{\mathbf{f}}_{\mathrm{RF},l}$ be $\mathbf{f}_{\mathrm{RF},l}$ without the n:th element and letting $\mathbf{G}_l(n,:)$ be the n:th row of $\mathbf{G}_l$ and $\bar{\mathbf{G}}_{l,n}$ be the matrix $\mathbf{G}_l$ with the n:th row excluded.

$$|\mathbf{w}_{\mathrm{RF},l}^H \mathbf{G}_l \mathbf{f}_{\mathrm{RF},l}| = |\mathbf{w}_{\mathrm{RF},l}^H \bar{\mathbf{G}}_{l,n} \bar{\mathbf{f}}_{\mathrm{RF},l} + \mathbf{w}_{\mathrm{RF},l}^H \mathbf{G}_l(n,:)\mathbf{f}_{\mathrm{RF},l}(n)|. \tag{4.6}$$

Since everything is kept fix except for $\mathbf{f}_{\mathrm{RF},l}(n)$, the expression in Equation 4.6 is maximized if they are in phase, so the phase of $\mathbf{f}_{\mathrm{RF},l}(n)$ is chosen to achieve this. As such, the element is set as follows

$$\omega_{n,l}^{(1)} = \angle\left(\mathbf{w}_{\mathrm{RF},l}^H \bar{\mathbf{G}}_{l,n} \bar{\mathbf{f}}_{\mathrm{RF},l}\right); \quad \omega_{n,l}^{(2)} = \angle\left(\mathbf{w}_{\mathrm{RF},l}^H \mathbf{G}_l(n,:)\right), \tag{4.7}$$

$$\mathbf{F}_{\mathrm{RF}}(n,l) = \mathbf{f}_{\mathrm{RF},l}(n) = \frac{1}{\sqrt{N_t}} \exp\left[j(\omega_{n,l}^{(1)} - \omega_{n,l}^{(2)})\right]. \tag{4.8}$$

Optimizing $\mathbf{w}_{\mathrm{RF},l}$ is handled similarly, letting $\bar{\mathbf{w}}_{\mathrm{RF},l}$ be $\mathbf{w}_{\mathrm{RF},l}$ without the m:th element, letting $\mathbf{G}_l(:,m)$ be the m:th column of $\mathbf{G}_l$ and $\bar{\mathbf{G}}_{l,m}$ be $\mathbf{G}_l$ excluding the m:th column. The expression can be written as

$$|\mathbf{w}_{\mathrm{RF},l}^H \mathbf{G}_l \mathbf{f}_{\mathrm{RF},l}| = |\bar{\mathbf{w}}_{\mathrm{RF},l}^H \bar{\mathbf{G}}_{l,m} \mathbf{f}_{\mathrm{RF},l} + \mathbf{w}_{\mathrm{RF},l}^H(m) \mathbf{G}_l(:,m)\mathbf{f}_{\mathrm{RF},l}|. \tag{4.9}$$

The element in question is then maximized by setting it to

$$\omega_{n,l}^{(3)} = \angle\left(\bar{\mathbf{w}}_{\mathrm{RF},l}^H \bar{\mathbf{G}}_{l,m} \mathbf{f}_{\mathrm{RF},l}\right), \quad \omega_{n,l}^{(4)} = \angle\left(\mathbf{G}_l(:,m)\mathbf{f}_{\mathrm{RF},l}\right), \tag{4.10}$$

$$\mathbf{W}_{\mathrm{RF}}(m,l) = \mathbf{w}_{\mathrm{RF},l}(m) = \frac{1}{\sqrt{N_t}} \exp\left[j(\omega_{n,l}^{(4)} - \omega_{n,l}^{(3)})\right]. \tag{4.11}$$

After all columns have been treated, the algorithm is repeated until the change in $|\mathbf{W}_{\mathrm{RF}}^H \mathbf{H} \mathbf{F}_{\mathrm{RF}}|$ is below some threshold value. Now, the baseband weights in the digital precoding and combining can be determined from $\mathbf{W}_{\mathrm{RF}}$ and $\mathbf{F}_{\mathrm{RF}}$. First, the equivalent channel matrix can be formed as $\mathbf{H}_{\mathrm{eq}} = \mathbf{W}_{\mathrm{RF}}^H \mathbf{H} \mathbf{F}_{\mathrm{RF}}$. This represents the path from a transmitter RF chain to a receiver RF chain. For transmission of several data streams to a single user, finding the eigenvectors to the equivalent channel equates to finding independent directions of transmission, to avoid interference. Therefore, the baseband precoding can be found by taking the right eigenvectors, found by SVD of $\mathbf{H}_{\mathrm{eq}}$. This is written as $\mathbf{H}_{\mathrm{eq}} = \mathbf{U}\mathbf{\Sigma}\mathbf{V}^H$. The digital precoder and combiners is then constructed as

$$\mathbf{F}_{\mathrm{B}} = \beta \mathbf{V}\mathbf{P}; \quad \mathbf{W}_{\mathrm{B}} = \left(\mathbf{H}_{\mathrm{eq}} \mathbf{F}_{\mathrm{B}} \mathbf{F}_{\mathrm{B}}^H \mathbf{H}_{\mathrm{eq}}^H + \sigma^2 \mathbf{W}_{\mathrm{RF}}^H \mathbf{W}_{\mathrm{RF}}\right)^{-1} \mathbf{H}_{\mathrm{eq}} \mathbf{F}_{\mathrm{B}}, \tag{4.12}$$

where the matrix $\mathbf{P}$ can be calculated with the waterfill method. It was implemented in MATLAB using the `waterfill` function. The scalar β is used in order to normalize the transmitted power, and set to $\beta = \sqrt{N_s}/\|\mathbf{F}_{\mathrm{RF}}\mathbf{V}\mathbf{P}\|_F$.
For multiple users, the channel matrix is formed as described in Section 3.1. Then, the analog precoding weights are calculated in the same way as for the single-user case, where the channel matrix being several channel matrices combined lets the digital precoding be determined for every part corresponding to a certain user. On the

receiver side, each user is treated separately. The matrix $\mathbf{W}_{\mathrm{RF},k}$ can be calculated independently for each user. The total combining matrix used in the simulations is block diagonal where each block is made up of the weights for each user. To calculate the digital precoding weights, the block diagonalization algorithm described in Section 4.1 is used with an equivalent channel defined as $\hat{\mathbf{H}} = \mathbf{W}_{\mathrm{RF}}^H \mathbf{H} \mathbf{F}_{\mathrm{RF}}$.

4.3 FPS-AltMin Algorithm

The FPS-AltMin algorithm [1] is a special case of the AltMin algorithms developed by the authors in a previous article [7], developed for group mapping with the FPS approach as described in Section 2.4. This algorithm optimizes the baseband and the RF precoding together, as opposed to the split up method in Section 4.2. Using N_c multi-channel phase shifters and a network of switches decouples the RF precoding matrix into a binary matrix, representing the switch states, and a constant phase matrix. The problem now lies in optimizing the baseband precoding matrix and the binary switch matrix.
If the optimal precoding matrix, $\mathbf{F}_{\mathrm{opt}}$, is found using unconstrained digital precoding, then it was shown that the baseband and RF precoders that minimize the distance to $\mathbf{F}_{\mathrm{opt}}$ approximately result in the highest spectral efficiency. In other words, the following problem formulation can be used

$$\min_{\mathbf{F}_{\mathrm{RF}},\mathbf{F}_{\mathrm{B}}} \|\mathbf{F}_{\mathrm{opt}} - \mathbf{F}_{\mathrm{RF}}\mathbf{F}_{\mathrm{B}}\|_F = \|\mathbf{F}_{\mathrm{opt}} - \alpha \mathbf{S}\mathbf{C}\mathbf{F}_{\mathrm{DD}}\|_F. \tag{4.13}$$

The baseband precoding matrix is rewritten as $\mathbf{F}_{\mathrm{B}} = \alpha \mathbf{F}_{\mathrm{DD}}$, where $\mathbf{F}_{\mathrm{DD}}$ is a unitary matrix, $\mathbf{F}_{\mathrm{DD}}^H \mathbf{F}_{\mathrm{DD}} = \mathbf{I}_{N_s}$, and α is a scalar constant. The RF precoding is also rewritten as $\mathbf{F}_{\mathrm{RF}} = \mathbf{S}\mathbf{C}$ where $\mathbf{S} \in \{0,1\}^{N_t \times N_c N_t^{\mathrm{RF}}}$ is the binary switch matrix, and the phases of the fixed phase shifters are contained in $\mathbf{C}$. It is constructed as a block diagonal matrix where a vector $\mathbf{c}$ containing the phases is repeated N_t^{RF} times. The phase vector is written as

$$\mathbf{c} = \frac{1}{\sqrt{N_c}} \left[\mathrm{e}^{j\theta_1}, \ldots, \mathrm{e}^{j\theta_{N_c}} \right]. \tag{4.14}$$

Here, the phases are found by dividing the interval $[0,2\pi)$ evenly. Now, the objective function can be rewritten and an upper bound found to simplify the analysis, with details found in [1]

$$\min_{\alpha,\mathbf{S},\mathbf{F}_{\mathrm{DD}}} \alpha^2 \|\mathbf{S}\|_F^2 - 2\alpha \Re \left[\mathrm{tr} \left(\mathbf{F}_{\mathrm{DD}} \mathbf{F}_{\mathrm{opt}}^H \mathbf{S}\mathbf{C} \right) \right]. \tag{4.15}$$

Now, as the name of the algorithm hints, $\mathbf{F}_{\mathrm{DD}}$ is kept fix while α and $\mathbf{S}$ are updated. By adding a constant term, the problem can be expressed as

$$\min_{\alpha,\mathbf{S}} \|\Re \left(\mathbf{F}_{\mathrm{opt}} \mathbf{F}_{\mathrm{DD}}^H \mathbf{C} \right) - \alpha \mathbf{S}\|_F^2. \tag{4.16}$$

The optimal α is found by first vectorizing the first matrix into
$\mathbf{x} = \mathrm{vec} \left(\Re \left(\mathbf{F}_{\mathrm{opt}} \mathbf{F}_{\mathrm{DD}}^H \mathbf{C} \right) \right)$. The elements are then sorted into a vector denoted as $\tilde{\mathbf{x}}$,

with n elements in total. Define an interval $\mathcal{R}_i$ as $\mathcal{R}_i = [2\tilde{x}_i, 2\tilde{x}_{i+1}]$. Then, construct the following vector

$$\bar{x}_i = \begin{cases} \frac{1}{i}\sum_{j=1}^{i} \tilde{x}_j & \text{if } \bar{x}_i < 0 \text{ and } \bar{x}_i \in \mathcal{R}_i, \\ \frac{1}{n-i}\sum_{j=i+1}^{n} \tilde{x}_j & \text{if } \bar{x}_i > 0 \text{ and } \bar{x}_i \in \mathcal{R}_i, \\ +\infty & \text{otherwise.} \end{cases} \tag{4.17}$$

It turns out that at most 5 elements in $\bar{\mathbf{x}}$ are finite [1]. Out of the finite elements, each is passed to a function $f(\bar{x}_i)$, and it turns out that the optimal α is given directly as $\alpha^* = \arg\min_{\bar{x}_i} f(\bar{x}_i)$. The function in question is defined to be

$$f(\alpha) = \|\tilde{\mathbf{x}} - \alpha\mathbf{s}\|_2^2 = \begin{cases} i\alpha^2 - 2\sum_{j=1}^{i} \tilde{x_j}\alpha + \sum_{j=1}^{n} \tilde{x}_j^2 & \text{for } \alpha < 0 \text{ and } \alpha \in \mathcal{R}_i, \\ (n-i)\alpha^2 - 2\sum_{j=i+1}^{n} \tilde{x_j}\alpha + \sum_{j=1}^{n} \tilde{x}_j^2 & \text{for } \alpha > 0 \text{ and } \alpha \in \mathcal{R}_i. \end{cases} \tag{4.18}$$

Knowing the optimal α, the optimal switch matrix can be determined as

$$\mathbf{S}^* = \begin{cases} \mathbb{1}\left\{\Re(\mathbf{F}_{\text{opt}}\mathbf{F}_{\text{DD}}^H\mathbf{C}^H) > \frac{\alpha^*}{2}\mathbf{1}_{N_t \times N_c N_t^{\text{RF}}}\right\} & \alpha^* > 0, \\ \mathbb{1}\left\{\Re(\mathbf{F}_{\text{opt}}\mathbf{F}_{\text{DD}}^H\mathbf{C}^H) < \frac{\alpha^*}{2}\mathbf{1}_{N_t \times N_c N_t^{\text{RF}}}\right\} & \alpha^* < 0. \end{cases} \tag{4.19}$$

With both α^* and $\mathbf{S}^*$ known, we can fix α and $\mathbf{S}$ to these values and update $\mathbf{F}_{\text{DD}}$. Since only $\mathbf{F}_{\text{DD}}$ is changed, the objective in Equation 4.15 can now be rewritten to

$$\max_{\mathbf{F}_{\text{DD}}} \alpha\Re\left[\text{tr}\left(\mathbf{F}_{\text{DD}}\mathbf{F}_{\text{opt}}^H\mathbf{S}\mathbf{C}\right)\right]. \tag{4.20}$$

Then, the expression to be maximized can be upper bounded as follows

$$\alpha\Re\left[\text{tr}\left(\mathbf{F}_{\text{DD}}\mathbf{F}_{\text{opt}}^H\mathbf{S}\mathbf{C}\right)\right] \leq \left|\text{tr}\left(\alpha\mathbf{F}_{\text{DD}}\mathbf{F}_{\text{opt}}^H\mathbf{S}\mathbf{C}\right)\right| \leq \|\mathbf{F}_{\text{DD}}^H\|_\infty \|\alpha\mathbf{F}_{\text{opt}}^H\mathbf{S}\mathbf{C}\|_1. \tag{4.21}$$

The second inequality is exact for $\mathbf{F}_{\text{DD}}^* = \mathbf{V}_1\mathbf{U}^H$, which are given by SVD; $\alpha\mathbf{F}_{\text{opt}}^H\mathbf{S}\mathbf{C} = \mathbf{U}\mathbf{\Sigma}\mathbf{V}_1^H$. With all variables determined, the algorithm now calls to repeat this calculation until it converges. This was interpreted as repetition until the expression in Equation 4.15 changes little enough between iterations. Then, recreate the baseband precoding as $\mathbf{F}_{\text{B}} = \alpha\mathbf{F}_{\text{DD}}$. In the multi-user case, the same block diagonalizaton as done in Section 4.2 is repeated to minimize interference. This returns $\mathbf{F}_{\text{BD}}$, which is multiplied with the determined baseband precoding matrix to cancel out interference.

On the receiver side, the procedure is the same. In the multi-user case, the combining matrices of each user is as in Section 4.2 treated seperately and then combined to form a block diagonal matrix.

The normalization factor is then calculated as

$$\kappa = \frac{KN_s}{\|\mathbf{SCF}_{\mathrm{B}}\mathbf{F}_{\mathrm{BD}}\|_F^2}. \tag{4.22}$$

For the single user case, the block diagonalization matrix is omitted as no interference needs to be cancelled. Finally, the baseband precoding matrix is $\mathbf{F}_{\mathrm{BB},k} = \sqrt{\kappa}\mathbf{F}_{\mathrm{B},k}\mathbf{F}_{\mathrm{BD},k}$, and the RF precoding matrix is $\mathbf{F}_{\mathrm{RF}} = \mathbf{SC}$. Details and proofs can be found in [1].

4.4 LASSO-AltMin Algorithm

The LASSO-AltMin is similar in approach to the FPS-AltMin algorithm, but intended to use with a so-called double phase shifter structure [3]. As is explained in more detail in Section 2.5, a single phase shifter with amplitude control can be used instead, with some reservations for differences when using quantized phase shifters. In this thesis, the DPS algorithm is used but with intentions to realize it with a single phase shifter with amplitude control instead of two phase shifters working in parallel.
The minimization problem is expressed similarly to Equation 4.13, specifically as:

$$\min_{\mathbf{F}_{\mathrm{RF}},\mathbf{F}_{\mathrm{B}}} \|\mathbf{F}_{\mathrm{opt}} - \mathbf{F}_{\mathrm{RF}}\mathbf{F}_{\mathrm{BB}}\|_F, \qquad |(\mathbf{F}_{\mathrm{RF}})_{i,j}| < 2,\ \|\mathbf{F}_{\mathrm{RF}}\mathbf{F}_{\mathrm{BB}}\|_F^2 \leq KN_s, \tag{4.23}$$

for K users. The relaxed condition on $\mathbf{F}_{\mathrm{RF}}$ comes from the combination of two phase shifters. It is given in [3] that the optimal precoder can always be perfectly decomposed into an analog and a digital precoder for the minimal number of phase shifters, $N_t^{\mathrm{RF}} = KN_s$, which is special for the DPS structure and due to the relaxed amplitude conditions. As the algorithm uses alternating minimization, the analog precoder is considered at first. This is seen to become a LASSO problem, which stands for least absolute shrinkage and selection operator, and rewrites the objective function to only use a subset of the variables. As in the FPS-AltMin algorithm, semi-orthogonal constraints are enforced on the baseband precoder, i.e. forcing $\mathbf{F}_{\mathrm{BB}}\mathbf{F}_{\mathrm{BB}}^H = \mathbf{I}_{N_t^{\mathrm{RF}}}$. The optimization problem in 4.23 has a closed form solution if semi-orthogonality is enforced, where the optimal analog precoder can be written as

$$\mathbf{F}_{\mathrm{RF}}^* = \mathbf{F}_{\mathrm{opt}}\mathbf{F}_{\mathrm{BB}}^H - \exp\left[\mathrm{angle}(\mathbf{F}_{\mathrm{opt}}\mathbf{F}_{\mathrm{BB}}^H)\right] \cdot (|\mathbf{F}_{\mathrm{opt}}\mathbf{F}_{\mathrm{BB}}^H| - 2)^+, \tag{4.24}$$

where the multiplication in the second term is elementwise, and $A^+ = \max(A,0)$. The next step is to calculate the digital weights, simply given by $\mathbf{F}_{\mathrm{BB}} = \mathbf{V}\mathbf{U}_1^H$ where $\mathbf{V}$ and $\mathbf{U}_1$ come from the SVD of $\mathbf{F}_{\mathrm{opt}}^H\mathbf{F}_{\mathrm{RF}}$, $\mathbf{F}_{\mathrm{opt}}^H\mathbf{F}_{\mathrm{RF}} = \mathbf{U}_1\mathbf{S}\mathbf{V}$. In the multi-user case, the same procedure as before holds. The precoding weights are calculated as in the single-user case, now with a composite channel matrix and the combining weights are handled seperately for each user. To cancel inter-user interference, the block diagonalization algorithm [26] is applied as before.

4.5 Wu (2018) Algorithm

This quite straight-forward algorithm was proposed in [4] for broadband systems with multiple users. The article describes both a procedure for phase shifters with

and without amplitude control, but only amplitude constrained phase shifters were considered in the implementation in this thesis.
The method described is simular to the method in Section 4.1. First, the optimal combining weights are taken as the N_r^{RF} first left eigenvectors of the channel matrix for each user, found through SVD. The total combining weights is then set to be a block diagonal matrix with the individual user matrices on the diagonal. Next, form the equivalent channel as $\tilde{\mathbf{H}} = \mathbf{W}_{\mathrm{RF}}^H \mathbf{H}$. As the base station architecture in general is considered to be group connected, a subset of $\tilde{\mathbf{H}}$ corresponding to the group size is selected. Let $\beta = N_t^{\mathrm{RF}}/\eta$ and $\zeta = N_t/\eta$ be the dimensions of the group and call the group channel matrix $\tilde{\mathbf{H}}_{\zeta,\beta}$. Then, to set the analog weights of this group, take the β first right eigenvectors of $\tilde{\mathbf{H}}_{\zeta,\beta}$, again through SVD.
As the phase shifters were set to be amplitude constrained, the constrained amplitude is enforced by simply taking the phase of the analog weights above, and set the amplitude to a constant $1/\sqrt{N_t}$ for the transmitter and $1/\sqrt{N_r}$ for the receiver. Next, use the block diagonalization described in Section 4.1 to cancel interference between users for the multi-user case. As no other digital weighting is specified and the algorithm was written for the multi-user MIMO case, it was elected in this work to add nothing in the digital domain for the single-user case.

4.6 Orthogonal Matching Pursuit (OMP)

This algorithm was presented in [5] and was been implemented in the Phased Array System Toolbox in MATLAB, as `omphybweights`. This instance of the algorithm is only available for fully connected systems. The idea is to build a codebook and pick columns of the RF precoding matrix from this codebook. The candidates can for example be the array response vectors of the channel. More precisely, the columns of the optimal precoder, $\mathbf{F}_{\mathrm{opt}}$ can be written as linear combinations of the vectors $\mathbf{a}_t(\phi_{i,l}^t, \theta_{i,l}^t)$ where $\phi_{i,l}^t$ and $\theta_{i,l}^t$ are the departure angles for all of the paths in the channel, and $\mathbf{a}_t$ is the array response. This was be constructed by letting $\mathbf{F}_{\mathrm{RF}}$ be made up of response vectors. The baseband weights were set to let the total precoding matrix $\mathbf{F}_{\mathrm{RF}}\mathbf{F}_{\mathrm{BB}}$ approximate $\mathbf{F}_{\mathrm{opt}}$ as good as possible [5].

4.7 Generalizing to multiple subcarriers

Out of the included algorithms, FPS [1], DPS [3] and Wu (2018) [4] included support for ODFM systems, while Hu (2019) [2] was generalized with the other algorithms as inspiration. In general, the RF weights were found using the method described for a single carrier, with the average over the channels for each subcarrier taken as the channel matrix. This needs to be done since the different frequencies are transmitted simultaneously and the phase shifters, implemented in the hardware, ideally provide the same phase shift over the entire bandwidth. Meanwhile, the digital precoding is before the transformation to time domain by the DACs, so different weights can be applied to each subcarrier. Therefore, the total matrix of baseband weights is given as

$$\mathbf{F}_{\mathrm{BB}} = [\mathbf{F}_{\mathrm{BB},1}, \ldots, \mathbf{F}_{\mathrm{BB},F}], \tag{4.25}$$

where $\mathbf{F}_{\mathrm{BB},f}$ denotes the precoding for the f:th subcarrier, and $\mathbf{W}_{\mathrm{BB}}$ is written correspondingly.

4.8 Summary of algorithms

In order to provide a more cohesive summary of the used algorithms, they are presented in broad strokes in Table 4.1.

Table 4.1: Overview of implemented algorithms for calculating the analog and digital precoding and combining weights.

Algorithm	Optimization method	Phase shifter implementation
Optimal	Closed form	-
Hu (2019) [2]	Element-wise	PS w/o amplitude control
Wu (2018) [4]	Closed form	PS w/o amplitude control
FPS [1]	AltMin	Fixed PS and switch network
DPS [3]	AltMin	PS with amplitude control
OMP [5]	Codebook based	PS w/o amplitude control

4.9 Example of hardware required for different algorithms

Based on the analysis of components presented in Section 2.6, the area, number of diodes and DC power consumption for each architecture can be estimated. As is clear from Table 4.1, the different tested algorithms require somewhat different hardware: the FPS algorithm uses its own structure, DPS requires amplitude control on the phase shifters, while the rest use regular phase shifters without amplitude control. In order to make the hardware estimation clearer, a fully connected example is presented in Table 4.2 for a base station with $N_t = 8$ antennas, $N_t^{\mathrm{RF}} = 2$ RF chains and $N_c = 5$ fixed phase shifters. The regular phase shifters have 4 bits to set the phase, while the amplitude control phase shifters have 6 bits for phase and 6 bits for amplitude. Only a transmitter is considered, while a real system may be a transceiver with higher complexity. In Mondal et al. (2018) [9], a fully connected receiver is presented with total chip area of 6.2 mm^2 and DC power consumption of 0.34 W. Here, phase control is done by controlling the amplitude of a real stream and an imaginary stream and summing them. This achieves the same end goal as changing the phase with a phase shifter, but the components would be different. Compared to the summed results in Table 4.2 for PS with amplitude control, the area and the power consumption are seen to be smaller in the real implementation. It's expected that the power consumed is smaller in a receiver than a transmitter as the power amplifier has a big contribution, but the area should be comparable.

Table 4.2: Example of calculations for hardware estimation following Section 2.6, for three fully connected systems. Area A is given in mm^2 and consumed DC power P_{dc} in W. Number of diodes is denoted N_d. The number of components needed for the architecture of a certain kind is N.

	FPS				**Regular PS**			
Attribute	N	A	P_{dc}	N_d	N	A	P_{dc}	N_d
RF chains	2	2.6	0.42	56	2	2.6	0.42	56
Phase shifters	80	5.4	0	0	16	1.1	0	320
Switches	80	0.8	0	1280	-	-	-	-
Combiner	40	11.2	0.4	80	8	2.2	0.08	16
Power amplifiers	8	4.7	2.3	192	8	4.7	2.3	192
Sum	-	24.7	3.1	1608	-	10.6	2.8	584
	Ampl. PS				**MIMO**			
Attribute	N	A	P_{dc}	N_d	N	A	P_{dc}	N_d
RF chains	2	2.6	0.42	56	8	10.4	1.7	224
Phase shifters	16	1	0.4	400	-	-	-	-
Combiner	8	2.2	0.08	16	-	-	-	-
Power amplifiers	8	4.7	2.3	192	8	4.7	2.3	192
Sum	-	10.5	3.2	664	-	15.1	4	416

5
Simulated Spectral Efficiency

In this section, the results from the investigations are presented and the consequences discussed. In Section 5.1 and 5.3 it is discussed which algorithm and hardware implementation is optimal for the single-user and multi-user case, respectively. In Section 5.2, results for the LOS case are presented for a single user system. Algorithm efficiency is investigated in Section 5.4. In Section 5.5, runtime is presented for each algorithm. Then, quantization of phase shifters is explored in Section 5.6, and the effect from adding an error to the channel matrix used to calculate weights is discussed in Section 5.7. Finally, results using a more realistic, measurement based channel model are presented in Section 5.8

5.1 Single-user System Comparisons

First, all implemented algorithms were used to compute analog and digital weights for a single-user, single carrier system. The SNR, defined as transmit power over receiver noise, was varied and the resulting spectral efficiency computed. In Figure 5.1, the results are presented for the investigated algorithms. The optimal hybrid beamforming algorithm is described in Section 4.1. Where applicable, the fully connected and partially connected cases have been simulated. Antenna arrays with $N_t = 64$ and $N_r = 16$ antennas were used and the number of RF chains were set to 4 for both transmitter and receiver, except for the MIMO case where $N_t^{\mathrm{RF}} = N_t$ and $N_r^{\mathrm{RF}} = N_r$. The used channel was cluster based with 16 scattering centers, each giving rise to 8 rays.
As expected, the fully digital MIMO system with 16 data streams achieved the highest spectral efficiency in Figure 5.1, and analog beamforming with only one stream resulted in the lowest. At SNR below $-25\,\mathrm{dB}$, single-stream transmission such as in analog beamforming gave the highest spectral efficiency. While the fully connected systems performed close to the optimal case, the partially connected algorithms still performed about twice as good as analog beamforming at an SNR of $0\,\mathrm{dB}$, and about as good or better than OMP run with a fully connected system. At an SNR of $30\,\mathrm{dB}$, a fully connected system achieved a spectral efficiency of $60\,\mathrm{bps/Hz}$. The partially connected systems reached $55\,\mathrm{bps/Hz}$ in the case of Hu, FPS and DPS, while Wu placed slighly lower at $51\,\mathrm{bps/Hz}$, where bps stands for bits per second. By applying a linear fit between $15\,\mathrm{dB}$ and $30\,\mathrm{dB}$ to the MIMO curve and the unconstrained hybrid beamforming curves respectively, the slopes were found to be $1.3\,\mathrm{bps/Hz/dB}$ for the hybrid beamforming systems and $4.3\,\mathrm{bps/Hz/dB}$ for the MIMO case. This difference comes from the MIMO instance having four

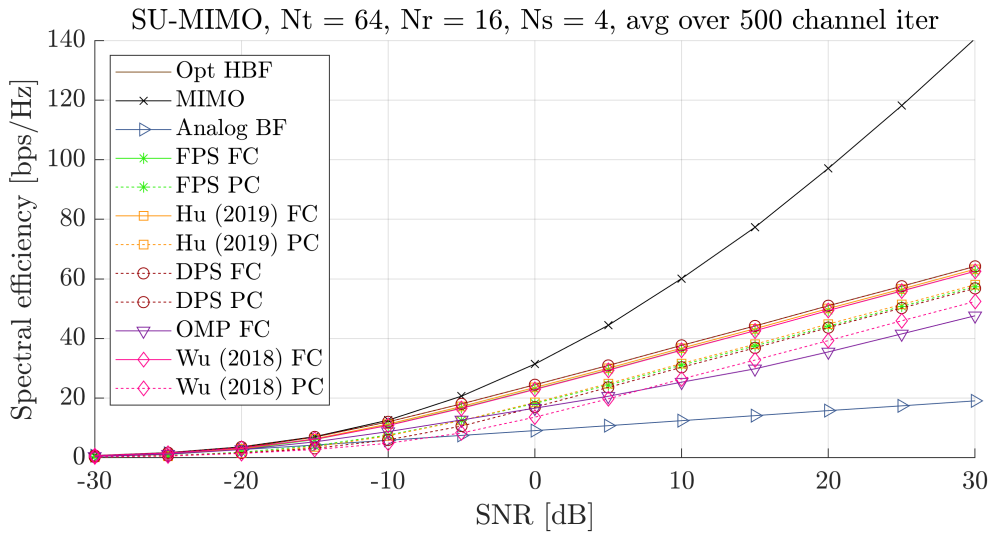

Figure 5.1: Comparison of spectral efficiency achieved with different algorithms. Where possible, both partially connected (PC) and fully connected (FC) systems have been used. The number of antennas were 64 at the transmitter and 16 at the receiver. The curves for DPS FC and optimal hybrid beamforming overlap completely.

times as many streams. The factor between the cases was not exactly four since the environment was not rich enough to support ideal MIMO transmission.

In order to observe the effect of the antenna array size, the number of RF chains were kept fixed at $N_t^{\mathrm{RF}} = N_t^{\mathrm{RF}} = 4$ and the receiver antennas kept at $N_r = 16$, then the number of transmitting antennas at the base station was varied from 32 to 128 in steps of 16. In general, N_t was not an even square, so in those cases the array was rectangular. Below 64 antennas, the shorter axis was set to 4 antennas, and above it was kept at 8 antennas. From the results in Figure 5.2, it seems as if the achieved spectral efficiency increased most dramatically for the MIMO-implementation. The flattest increase can be seen for analog beamforming. The hybrid beamforming algorithms experience roughly the same rate of increased spectral efficiency for increasing the number of antenna elements. The improved spectral efficiency with number of antennas is due to higher beamforming gain - as noted in Section 2.1, larger arrays offer narrower beams and higher gain in desired directions. This affected MIMO more, as it had a larger number of streams.

In order to answer how many antennas the UE needs, the equivalent investigation was done for N_r, testing from 8 receiver antennas to 56, in steps of 8. Again, the number of data streams in the case of hybrid beamforming was kept at $N_s = 4$, but increased in the MIMO case. This is because the smaller channel dimension was varied, which limits the number of allowed MIMO streams. The results are presented in Figure 5.3. Below 16 antennas, the number of antennas along the smaller dimension was kept at 2 and above, it was set to 4. The increase in spectral efficiency for MIMO would be expected to be higher since the number of streams increases with N_r. However, the number of clusters used in the simulation was $N_{\mathrm{cl}} = 16$, so the environment was not spatially diverse enough to allow many more

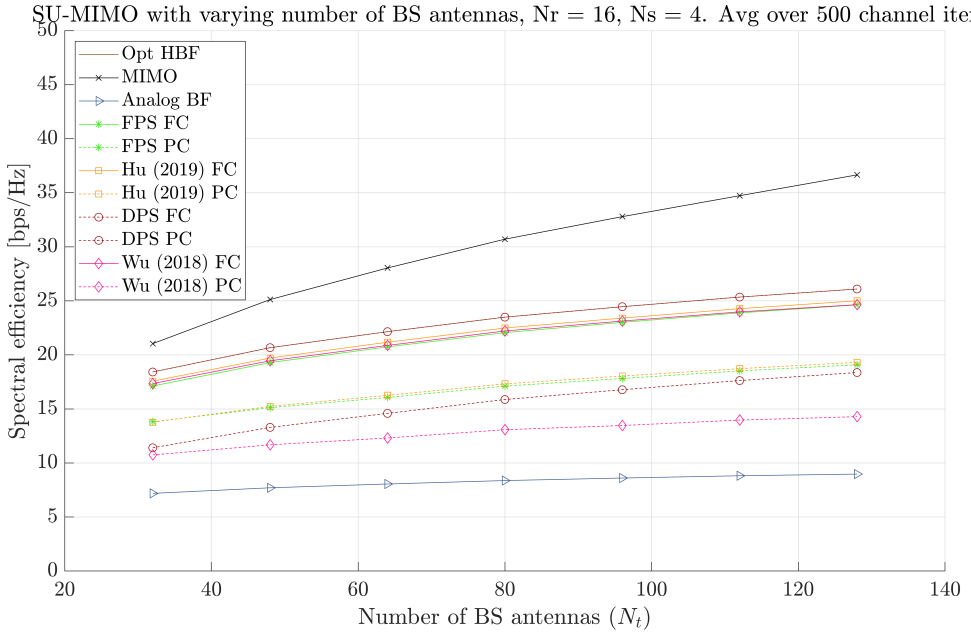

Figure 5.2: Spectral efficiency over number of base station antennas, for different algorithms. The results for DPS FC and optimal hybrid beamforming overlap completely.

strong, independent streams. Since waterfill was implemented, not all available streams were used. The streams corresponding to the weaker channel gains would not contribute much to the total spectral efficiency but draw power, so by enabling waterfill, the spectral efficiency is maximized even if it means turning off many streams. It was seen in this case that the number of transmitted streams varied depending on the channel instance, but was typically around 10 and did not exceed 16. This is an expected result, as $N_{\text{cl}} = 16$ and the number of clusters set the number of paths well separated in angle. The hybrid beamforming algorithms show the same behaviour as they did in Figure 5.2, showing that for an increase in spectral efficiency, either antenna array can be increased.

In addition to the single-carrier results provided previously, simulations were also done for OFDM systems with multiple subcarriers. A similar investigation as in Figure 5.1 over different receiver SNR values is presented in Figure 5.4. The OMP algorithm was not included due to uncertainty about how it was implemented for the multi-subcarrier case - the MATLAB documentation only cites a narrowband version. Analog beamforming was not added due to a need to rework some of the code and time limitations. Since spectral efficiency is normalized by bandwidth, it follows that the results are roughly in the order of the results in Figure 5.1. This system would however allow a much larger bandwidth, so the actual data rates in bps would be higher.

There are some slight differences for FPS, which is seen to perform a bit worse in the multi-subcarrier case. In the other algorithms, the mean of the channels is used to calculate the analog weights which are common over all frequencies. In FPS, the inner product of the frequency specific baseband weights and the optimal

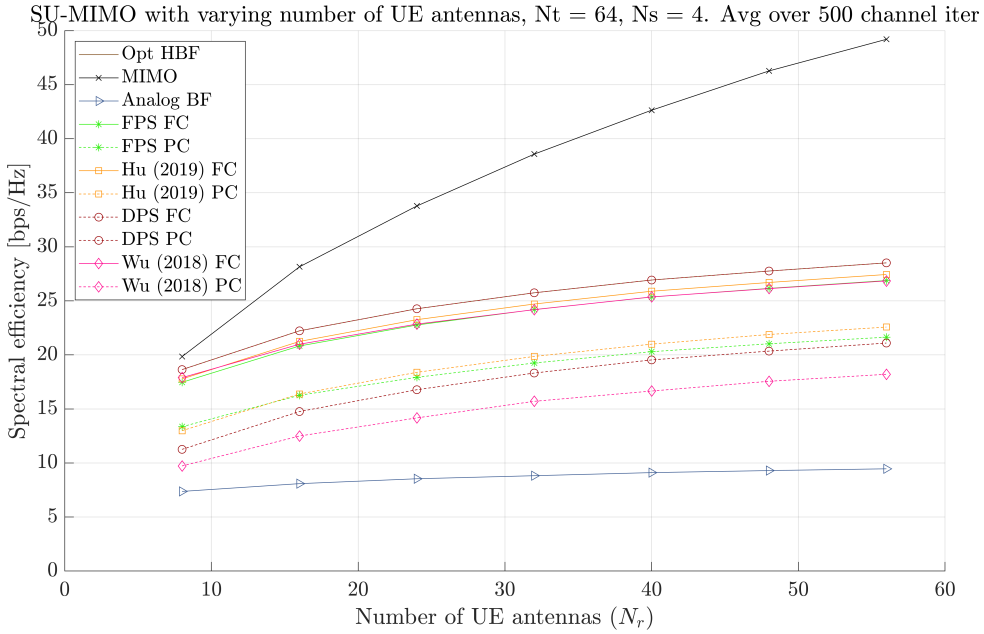

Figure 5.3: Spectral efficiency over number of user equipment antennas. The curves for DPS FC and optimal hybrid beamforming overlap completely.

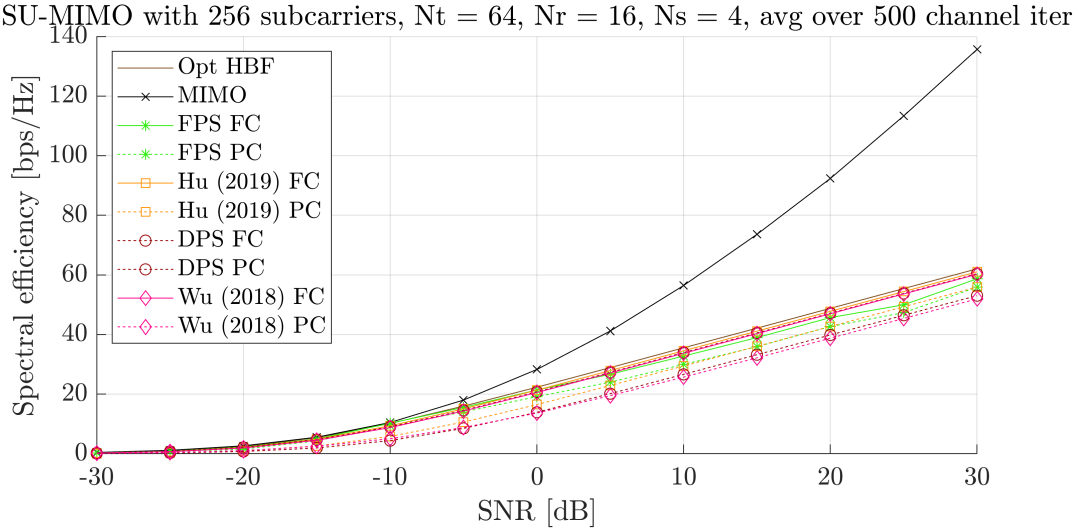

Figure 5.4: Comparison of weight algorithms simulated with 256 subcarriers.

weights is taken when determining the analog weights, which may behave slightly different than in the other cases. The FPS receiver weights were found to be poorly conditioned, so a small value was added the diagonal of the receiver weight matrix, to allow inversion. This then affects the spectral efficiency somewhat.

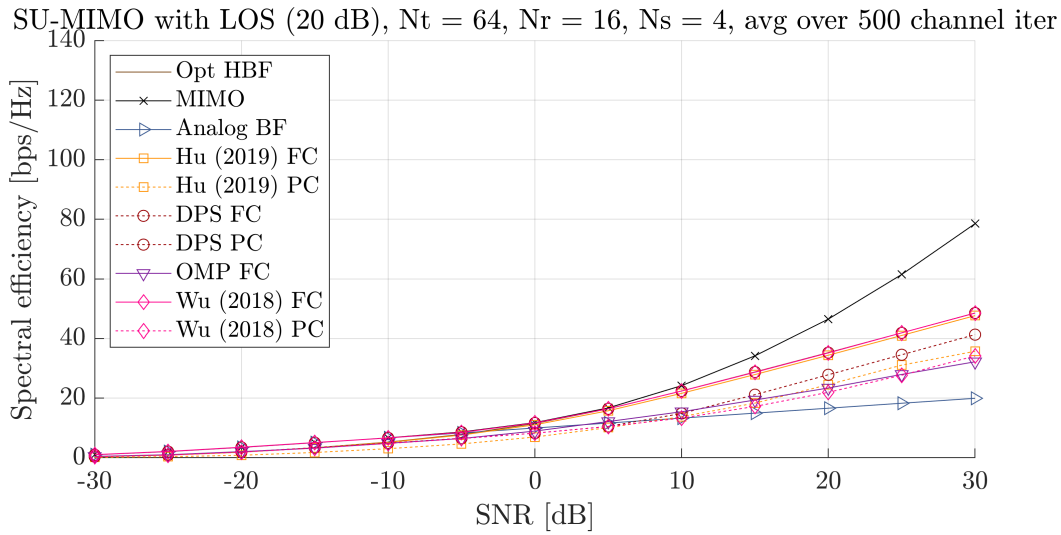

Figure 5.5: Algorithm comparison in the LOS case, where one path has 20 dB higher gain than the others. The curves for DPS FC and optimal hybrid beamforming are seen to overlap.

5.2 Line-of-Sight Investigations

In a real testing environment, it would be expected to sometimes have one path much stronger than the others. This was called the strong LOS case and tested by setting the gain of one path to 20 dB higher than the rest. The results are shown in Figure 5.5. DPS [3] and FPS [1] were found to give poorly conditioned weights in this case, causing numerical issues. For DPS, it could be solved by implementing waterfill, which was not included in the original algorithm. This was not sufficient in the FPS case, so it was excluded.
Due to channel normalization, the increased gain of one path comes at the cost of gain for the other paths which makes transmission there weaker. This leads to reduced diversity and lowers performance, especially in the MIMO case. Compared to the NLOS case in Figure 5.1, analog beamforming becomes more competitive, as it only uses one path regardless. If very small SNR is considered, it can be seen that the DPS algorithm with waterfill enabled follows the analog beamforming curve. When the power allocated to each stream is investigated, it confirms that only one data stream is used in that case.
If the LOS component is instead set to 10 dB stronger than the other multipath gains, the different cases look like in Figure 5.6. This will be referred to as the weak LOS case. Here, the resulting spectral efficiency is as in the NLOS case in Figure 5.1. This shows that one strong path can be tolerated and allow the algorithms to function as normal, but in the very strong gain difference case in Figure 5.5, the performance starts to change.

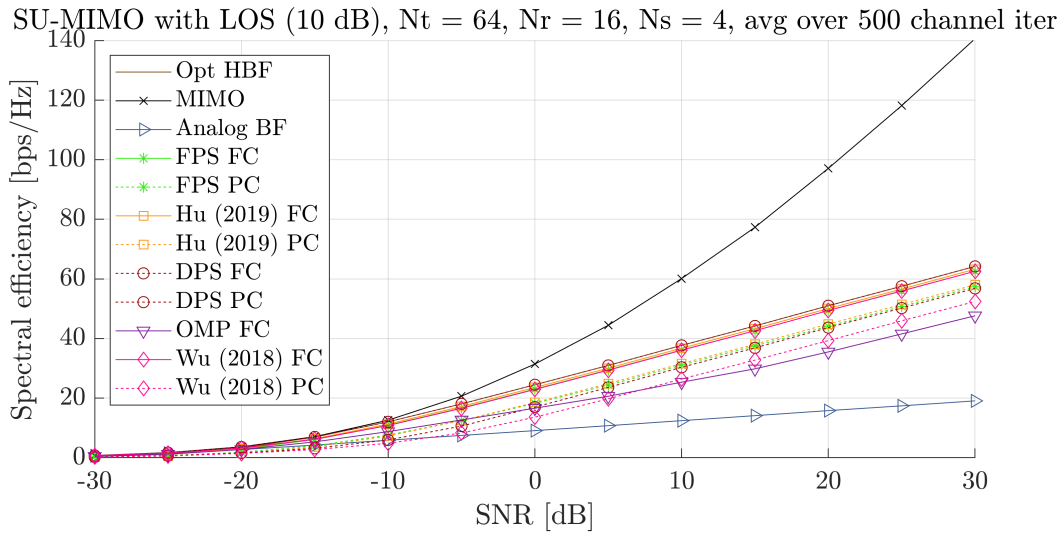

Figure 5.6: Algorithm comparison for LOS conditions, with one path gain set to 10 dB higher than the rest. Again, the curves for DPS FC and optimal hybrid beamforming overlap.

5.3 Multi-user System Comparisons

The used algorithms were also implemented in the multi-user case. Since analog beamforming is limited to single-user systems, it has not been included here. The OMP algorithm was also written for the single-user case [5]. There have been works to generalize this algorithm to a multi-user system [6], but this was only done for the case with one RF chain per receiver, so it was not pursued in this thesis.
The remaining algorithms are plotted in Figure 5.7 over SNR. Here, 64 transmitter antennas are used, each receiver has 4 antennas and there are in total 8 data streams transmitted to 4 non-collaborating users. The MIMO weights here are given by the function `blkdiagbfweights` which uses the block diagonalization algorithm described in Spencer (2004) [26]. The MIMO results presented in Figure 5.7 agree with the capacity given in the article.
In the same way as in the single-user case, everything was generalized to multiple subcarriers and an investigation over SNR was done, which is shown in Figure 5.8. As in the single-user case, the spectral efficiency is the same with one or multiple subcarriers as it is normalized over bandwidth. As in the single-user case, FPS is seen to degrade at high SNR for the multiple subcarrier case.

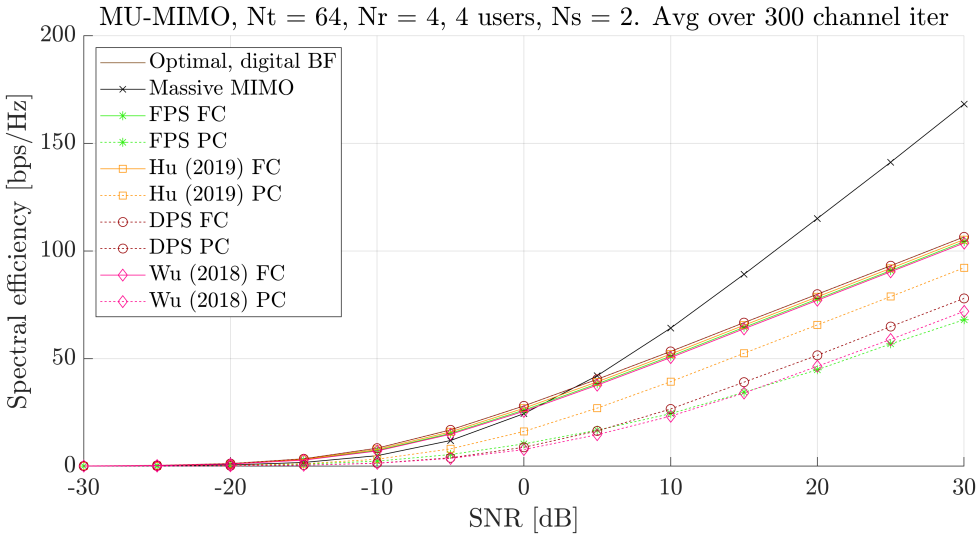

Figure 5.7: Comparison of investigated algorithms in the multiuser MIMO case. Each of the 4 users is equipped with 4 antennas and receives 2 data streams in the hybrid case. The curves for DPS FC and optimal hybrid beamforming overlap completely.

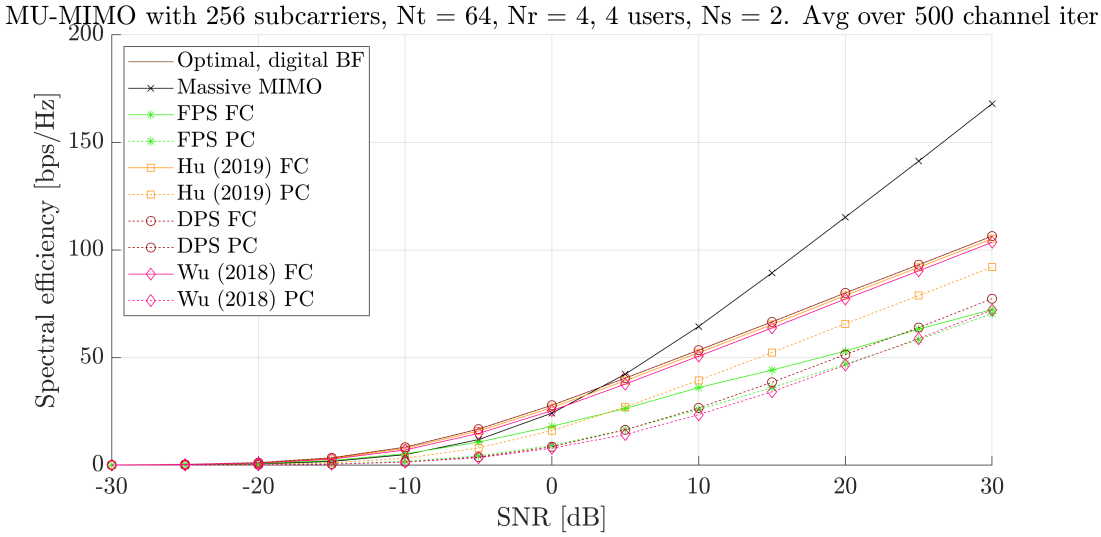

Figure 5.8: Comparison of investigated algorithms over SNR, in the multi-user, multi-subcarrier case. Here as well, the curves for DPS FC and optimal hybrid beamforming overlap completely.

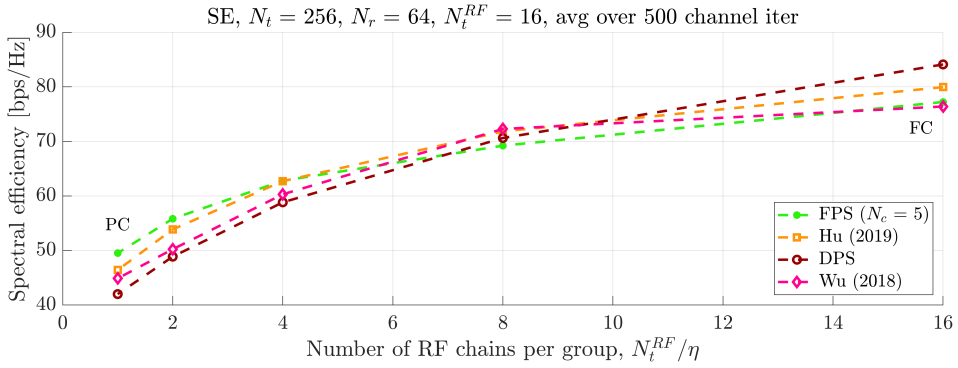

Figure 5.9: Spectral efficiency achieved using different algorithms and varying connectivity. The SNR was kept at 0 dB. 256 antennas were used at the transmitting base station and 64 were used at the receiver, and the number of RF chains were 16 at both.

5.4 Efficiency Investigations

In order to give a more in-depth understanding of how the connectivity between the RF chains and the antennas affect the spectral efficiency, a larger system was simulated with 256 antennas at the transmitter and 64 antennas at the receiver, and 16 RF chains at both. Then, the number of RF chain groups was varied, which is explained in Section 2.3. To keep the number of elements per group equal, the tested values for number of groups were {1,2,4,8,16}. The results are displayed in Figure 5.9. It can be seen that the spectral efficiency decreases gradually as the architectures go towards partially connected. This behaviour is expected, since the degrees of freedom decrease.
It is however a somewhat misrepresentative comparison, since all systems have different hardware components. To correct this, the complexity was estimated as the number of diodes or equivalent components. The efficiency as defined in Equation 2.4 was calculated for several architectures, as seen in Figure 5.10. The spectral efficiency data is the same as in Figure 5.9, but here it is divided by the number of diodes. Based on this, the algorithms from Wu (2018) [4] and Hu (2019) [2] perform best. Since the FPS architecture gives rise to a large number of switches who contain several diodes [22], the hardware saved on using fixed phase shifters ends up costly as can be seen from the poor efficiency.
While the number of diodes indicates system complexity, the area occupied on a chip is another aspect that relates to complexity. For example, inductors and delay lines are typically large components which are not caught by counting diodes. Chip area is also paramount to manufacturing cost. Therefore, the area was estimated for the different architectures and in Figure 5.11, the area-spectral efficiency is presented for different RF-to-antenna connectivities. Both these results and Figure 5.10 indicate that the spectral efficiency increase given by increasing the analog layer connectivity, does not outweigh the increased complexity of the system.
Another important factor when judging the efficiency is the consumed DC power, since base station power consumption is a major concern moving forward [28]. The estimated efficiency related to power consumption is shown in Figure 5.12. As in

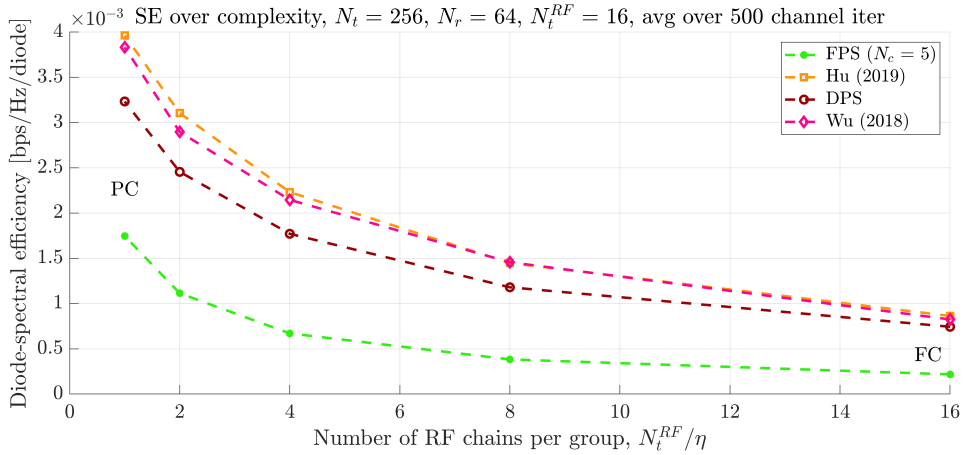

Figure 5.10: Efficiency of algorithms, referred to number of diodes in the architecture, over number of RF chains per group.

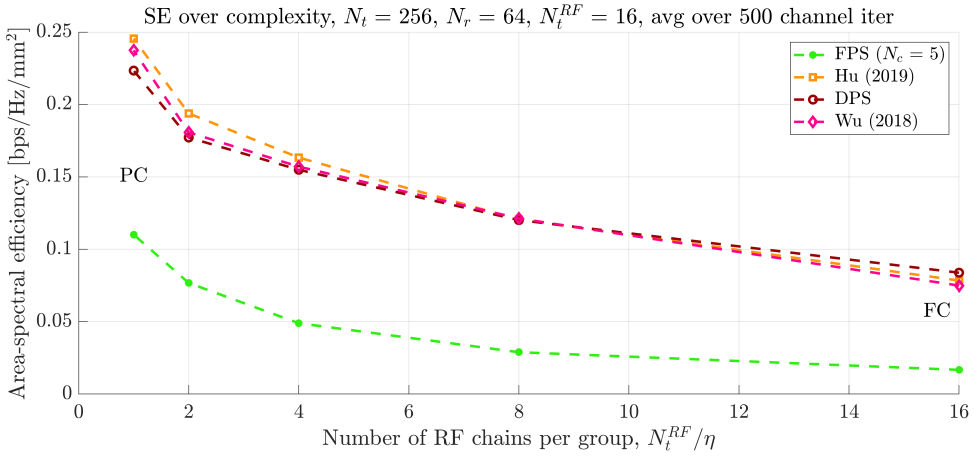

Figure 5.11: Efficiency referred to estimated chip area, for different algorithms over the number of RF chains per group.

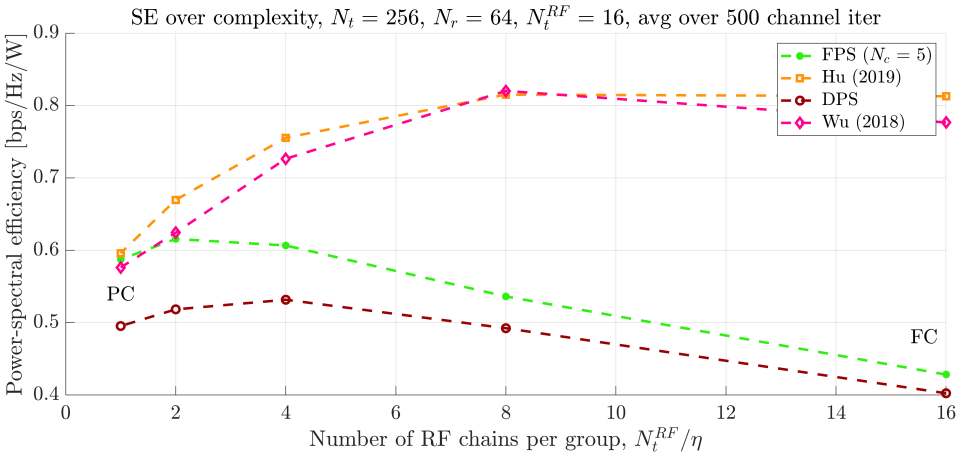

Figure 5.12: Efficiency of algorithms referred to consumed DC power.

the other cases, the algorithms presented by Wu [4] and Hu [2] seem to be the most power efficient. Interestingly, the spectral efficiency over power has a non-endpoint maximum. For Wu and Hu, this occurs when the 16 RF chains are divided into 2 groups. For FPS, the highest point is for 8 groups, and for DPS, it is for 4 groups. This investigation shows that from a power consumption perspective, it may be worth to consider a group connection at the transmitter.

5.5 Runtime Comparisons

Since the investigated algorithms for calculating precoding and decoding weights use different optimization strategies, the computation time in the simulations vary somewhat. A comparison of runtime statistics for each algorithm is presented in Figure 5.13. The algorithm runtime was measured in MATLAB for 500 different channels, then the tool `boxplot` was used to present the statistics of the measurements. Crosses represent outliers, the line in the box is the mean and the bottom and top of the box indicate the 25th and 75th percentiles respectively. As expected, Hu (2019) is slower than the rest of the algorithms due to calculating the weights elementwise in nestled loops. This may be a factor in choosing the best candidate, but it is also likely that the code can be rewritten to be brought up to speed with the rest. The higher the connectivity in the analog layer, the more of the RF precoding matrix is non-zero, which for Hu (2019) implies more computations as it otherwise skips zero entries. This results in the fully connected version being the slowest and the partially connected faster. The rest of the algorithms are roughly as fast as each other, but FPS and OMP are slower.

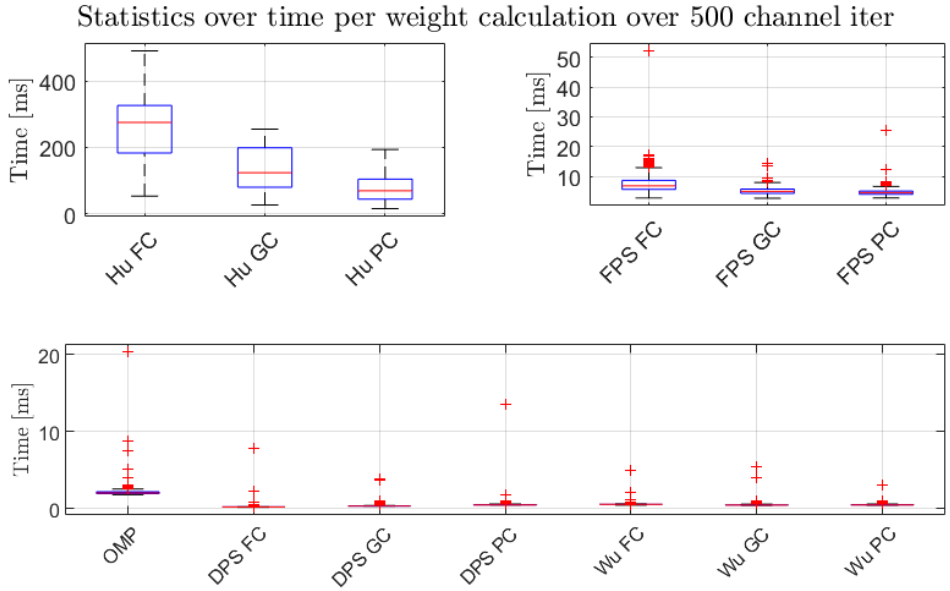

Figure 5.13: Runtime statistics for each algorithm. The number of base station antennas was set to $N_t = 64$, number of UE antennas was $N_r = 16$ and $N_s = 4$ streams were transmitted.

5.6 Effect of Quantized Phase Shifters

Since real phase shifters have limited resolution, the effect of resolution was investigated. The RF precoding matrices were elementwise replaced with the closest achieveable phase. The number of bits in the phase shifters control which phases are available, and this value was varied for each investigated SNR, here in the single user, single subcarrier case. The results are plotted in Figure 5.14. Since the FPS architecture utilizes fixed phase shifters, these were assumed to be designed in the hardware implementation and as such, suffer from no quantization effects. As expected, the spectral efficiency decreases with the number of bits. It should be noted that since the DPS algorithm uses both amplitude and phase control, and both aspects are quantized with the number of given bits. As such, DPS suffers more from decreased precision. Using a 2-bit phase shifter, the spectral efficiency decreased on average by approximately 14 % of the non-quantized value.

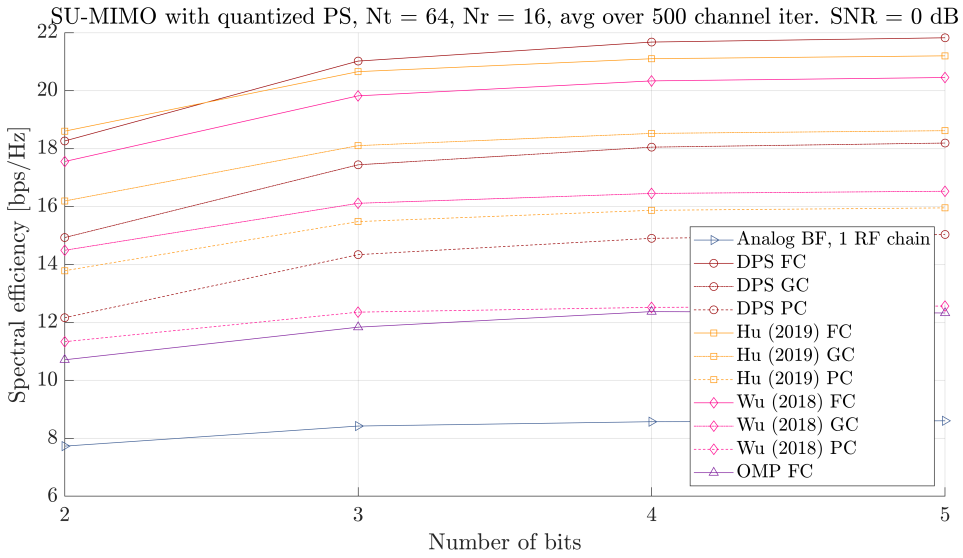

Figure 5.14: Comparison of spectral efficiency for different algorithms, over the number of bits in the quantized phase shifters. 4 RF chains are used on either side, 4 data streams are transmitted in parallel.

5.7 Effect of Errors in Channel Matrix

In a practical application, the channel matrix needs to be estimated for the investigated algorithms to work. Since this estimation likely results in some errors, simulations were done where the weights were calculated with matrices with an additive random error, as described in Section 3.1. The resulting normalized mean square error (NMSE) was calculated as the error variance was varied. The calculated spectral efficiency is plotted in Figure 5.15 for different NMSE values.

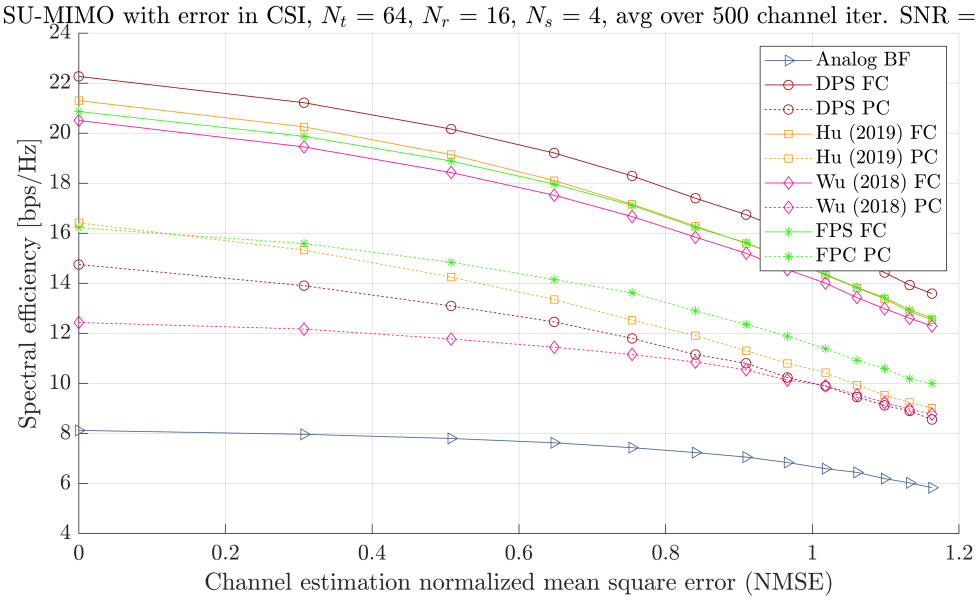

Figure 5.15: Spectral efficiency using weights calculated using channels with added error, for varying normalized mean squared error. The group connected (GC) architecture here has two RF chains per group.

5.8 Results Using a Measurement Based Channel

In addition to the cluster-based channel model, the channel was also calculated using the NYUSIM channel simulator, as described in Section 3.3. Both the LOS and the NLOS cases were tested with 400 iterations. Not all of the resulting channels were found to be suitable for simulations as they have been set up in this case. Here, rank deficient channels were removed in order to allow spatial multiplexing, so the effective number of simulations ended up being 151 for the LOS case presented in Figure 5.16, and 147 for the NLOS case in Figure 5.17. By looking at the individual path gains in the results used for computing the channel, it was found that in the LOS case, the difference between the LOS gain and the next highest gain was around 10 dB. Figure 5.6 shows LOS for the cluster based model with comparable difference in path gain. These results were also found to be comparable to the corresponding NLOS case. Similarly to the strong LOS case for a scatter based channel, the FPS algorithm was excluded since the receiver weights were found to be poorly conditioned.
A difference between the results in Figure 5.16 and 5.17, and the multi subcarrier case in Figure 5.4, is the MIMO performance. It is significantly lower when simulated with the NYUSIM channel, which comes from the lower amount of scatterers. By observing the waterfill power allocation, it was seen that around 14 diverse paths could be used with the scatter based channel, but only around 8 or 9 with the NYUSIM channel.

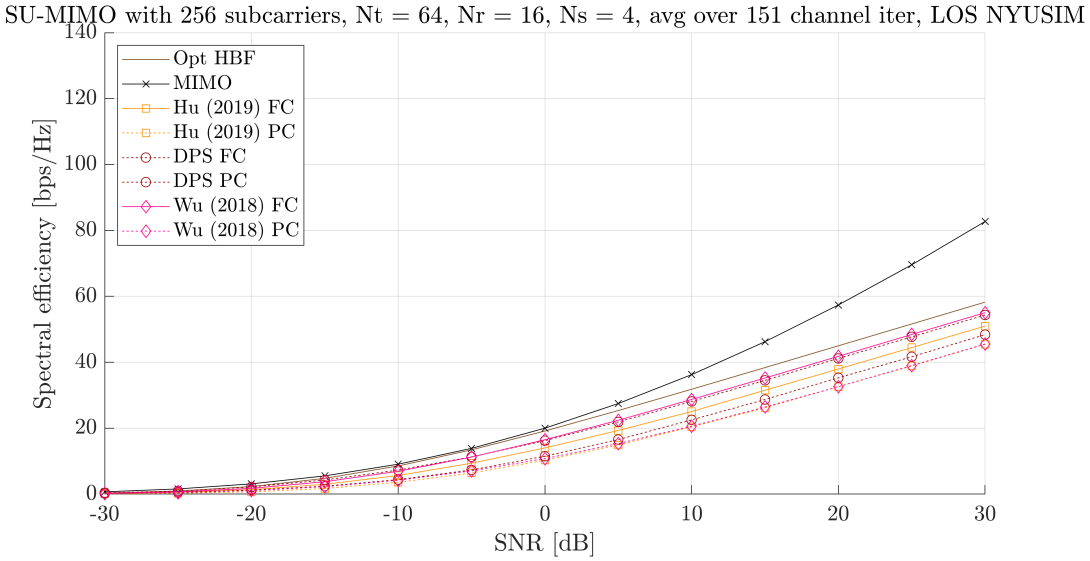

Figure 5.16: Simulation over SNR using a channel generated from the NYUSIM program set to LOS.

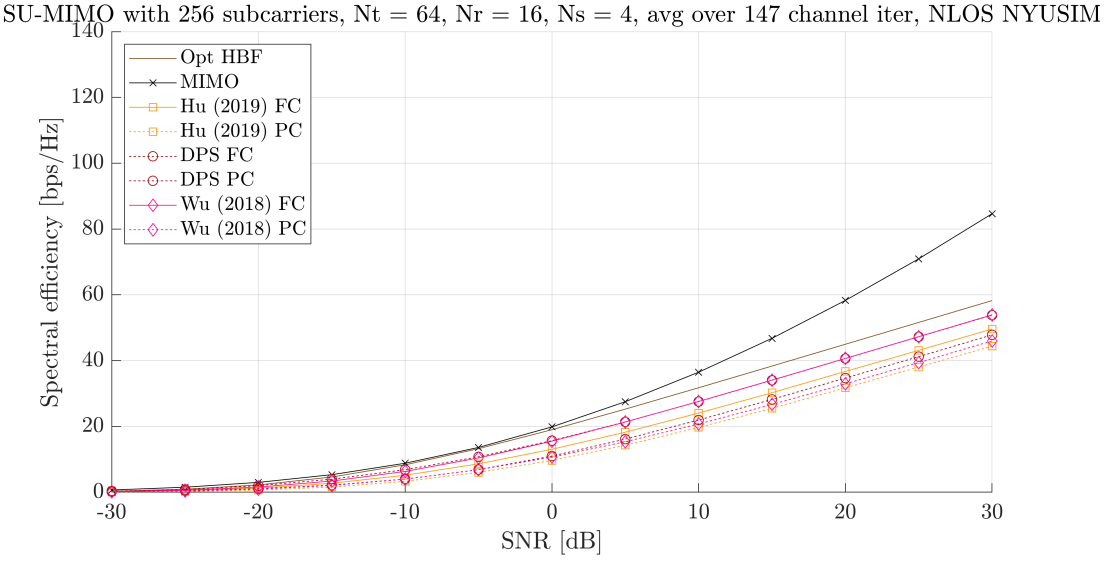

Figure 5.17: As in Figure 5.16, simulation over SNR using a channel derived from the NYUSIM program, set to NLOS.

6
Discussion

In this chapter, the used methods and results are discussed. The results from Chapter 5 are compared and analysed based on available literature. In addition, suggestions for future work are presented, and societal and environmental impact of the work is handled.

6.1 Method Analysis

It was seen in the simulations that it was required to have at least as many clusters as data streams, and at least as many scatterers in total as the lowest dimension of the channel matrix. In this investigation, the lowest channel dimension translates to the number of UE antennas. Based on measurement results, Samimi et al. [29] modelled a few dominant scatterers and found the rest to be weak. The used environment made up of typically around 10 to 16 clusters is likely too rich based on this. Although using very few scatterers resulted in numerical errors for particularly the LASSO-AltMin (DPS) and the FPS-AltMin (FPS) algorithms, it is more likely that these algorithms should be modified than that the channel should be set to contain enough scatterers. While the NYUSIM software generated channels had fewer scatterers in general, they were also in many cases rank deficient. Then, the smallest eigenvalues were not only small but zero. This breaks the assumptions of the algorithms and therefore, rank deficient channel matrices were excluded. Since these conditions may arise in a real measurement, more work should be put into handling these cases.

In the scatter based channel model, the channels at the different subcarriers were generated with the same gain and angles for the multipath components. The difference in the channels came only from having different signal wavelengths, thus experiencing a different element spacing. The antenna arrays were simulated with elements spaced a half wavelength at the center frequency. As the bandwidth was set to 400 MHz, the difference in element spacing was roughly 0.08 mm at the edge of the band, $f_{\max} = 28.2\,\text{GHz}$. This gives a quite small channel variation between subcarriers. One issue in OFDM systems is that many subcarriers share one phase shifter setting. If the channels are very similar, this doesn't cause much loss, as was the case in this thesis. Without accurate representation of the channel variations at different subcarriers, it is hard to draw conclusions for how the OFDM systems perform, as real systems exhibit stronger frequency dependance.

The estimation of the hardware data in Section 2.6 have some reservations. First, the technologies the components were built in varied slightly. However, all were

realized with a CMOS substrate, so although feature sizes varied between them, they should still be comparable. Second, a real system is more than the sum of its components, especially MMICs. This mainly affects the area estimation. However, the calculated area is not intended to predict the area in an implementation, but to compare between for example phase shifters with and without amplitude control. One could also argue that summing over core areas with some empty space is fair since integrated components either way require some spacing to avoid signal leakage.

6.2 Result Analysis

At the investigated SNR values, there is a clear benefit of employing several RF chains, especially when an SNR of up to 30 dB is considered. However, it should be kept in mind that at very low values, below -25 dB, analog beamforming with a single RF chains seems to dominate. In this region, the signal is too weak for spatial multiplexing to be beneficial [30, p. 347], so the simplest case of a single beam focused by the entire array performs best, which is done in the hybrid beamforming case when waterfill is implemented. In the investigations with a cluster based channel where a LOS component was included, analog beamforming performed better than hybrid beamforming up to roughly -10 dB. Since the dominating direction has higher gain, the other directions need more power until spatial multiplexing starts outperforming using all power to transmit in a single direction. Using waterfill on the implemented hybrid beamforming algorithms, they are seen to use only one RF chain at low SNR. At higher SNR, they start enabling multiple RF chains again to perform hybrid beamforming.
To analyze the different results found for the different LOS cases, consider the ratio between the largest and second largest eigenvalue. The eigenvalues of the channel matrix $\mathbf{H}$ relate to the gain of the orthogonal channels possible in the system and are ordered as $\nu_1 \geq \nu_2 \geq \cdots \geq \nu_m$ where m is the rank of the channel. The corresponding path power gains are ν_1^2, $\nu_2^2, \ldots, \nu_m^2$ [30]. The ratio ν_1/ν_2 is presented in Table 6.1 for the different channel realizations and conditions. From there, it can be seen that the difference between the biggest eigenvalues is comparable to the NLOS case when the path gain of the LOS component is about 10 dB higher than the other path gains. Using the cluster based model, it was also tested to set the path gain to 20 dB higher than the rest for LOS. This is seen in Table 6.1 to result is a much stronger gain difference. For this case, the results were also seen to differ from the NLOS and weaker LOS cases. A SE decrease of 13 bps/Hz was observed for HBF, and 55 bps/Hz for MIMO, which comes from the non-LOS paths being much weaker in the LOS case, which decreases the capability of spatial multiplexing.
From Table 6.1, it is also seen that for the NLOS and weaker LOS case, the NYUSIM generated channel has in both cases a higher ν_1/ν_2, which indicates more variation in the path gain. This follows what was observed in Section 6.1; the environment used in the NYUSIM software uses few scatterers with a lot of gain variation even in the NLOS case [29]. The number of multipaths was found to be around 30 from observing the output data and their gain had a standard deviation of 13 dB. For every channel calculation, the standard deviation of the roughly 30 multipath gains was taken, then this value was averaged over all iterations. Doing the same thing

in the scatter based channel case gave a mean standard deviation of 2.7 dB, so a less dominating maximum eigenvalue can be expected in the scatter based NLOS channel.

Table 6.1: Ratio of the largest channel eigenvalue, ν_1, over the second largest, ν_2. The ratio was determined for each channel instance, then averaged for 100 different channels. For a 10 dB stronger LOS component compared to the other multipaths, the eigenvalue ratio is not much bigger than in the NLOS case. When the LOS component is 20 dB stronger than the rest, the eigenvalue ratio is much higher.

ν_1/ν_2	NYUSIM	Scatter-based
NLOS	2.0	1.3
Weak LOS (10 dB)	2.2	1.5
Strong LOS (20 dB)	-	17.6

The FPS algorithm was found to have poorly conditioned weights in the LOS case and in the simulations with the NYUSIM generated channel. This can be explained by referring to Equation 4.19, where a locally optimal α is calculated and the switch network is set with this as the threshold. In the strong LOS case, the first columns of the optimal weights combined with the digital precoding weights have a much higher amplitude than the rest, so in many cases, the analog weights end up with most of the analog weights set to zero. This is problematic in the receiver, whose weights are inverted as seen in Equation 2.7. These numerical issues could likely be solved, but in this implementation, the algorithm was not suitable in the LOS case, or for investigations with a channel generated from the NYUSIM software.
It can be seen from the simulations over number of antennas in either the transmitter (Figure 5.2) or the receiver (Figure 5.3) that increasing either array size increases the spectral efficiency about as much for the hybrid beamforming solutions. This is expected, since increasing the array increases the gain at that user [30]. In Friis' equation, Equation 2.1, a gain increase at either end increases the received signal power equally.
For the BS antenna investigation (Figure 5.2), spectral efficiency increases more for the MIMO system than for HBF. This is due to having more data streams, here 16 compared to 4 in the HBF case. When the number of antennas increase, the beamforming gain increases which is reflected in an increase in value for all channel eigenvalues [30]. The effect is then stronger if more streams are used. Varying UE antennas (Figure 5.3), the spectral efficiency increased due to both increased beamforming gain, and from utilizing more streams. As noted in Section 5.1, the system cannot fully utilize the increase in avaliable streams, since there are not enough multipaths with sufficient path gain to support e.g. 56 streams. It was observed that around 10-16 streams were transmitted. The total spectral efficiency increase was therefore bigger than for increasing N_t, but not as big as it could potentially be in a very rich environment.
The results of the efficiency investigation depend on the assumptions done on the hardware, so the component choices matter. The components picked in this report were considered realistic choices and comparable to similar components found in the literature. In Section 4.9, the estimation is compared to a real, implemented receiver

presented in Mondal (2018) [9]. Comparing DC power, the calculated example consumes 3.2 W, and 0.9 W if power amplifiers are not included, while the reference receiver consumes 0.34 W [9]. There should be some power difference between a transmitter and a receiver, but even when removing the power amplifiers, the result is still higher. This shows that the model overestimates the necessary DC power, but the values are still in a somewhat reasonable range of each other. Considering area, Mondal [9] presents a total area including test structures of 6.2 mm^2 compared to the model result of 10.5 mm^2. There is likely some overestimation here from summing areas of components. Still, the values here are also reasonably close to each other. All in all, the model overestimates the complexity, but the results are still in range of a real system. Additionally, as noted in Section 6.1, the important thing is to compare the systems internally. Even if the total values are not in complete agreement with a real, fabricated system, conclusions can still be drawn on how partially connected systems perform compared to fully connected.

In the complexity and power efficiency investigations, the fully connected system performed worst out of the different architectures. To build a reasonably simple system with good performance, a group connected or partially connected architecture appears to be the best choice. In terms of power efficiency, the optimal architecture was found to be group connected. Looking at the values used to calculate total DC power, contributions from phase shifters and combiners were much smaller than from the power amplifiers and RF chains, as seen in Table 2.1 and for a specific architecture in Table 4.2. These components matter much more when area is considered, and how complicated the systems are to build. Since the power efficiency advantage was not seen to be very big over the partially connected solution, the best system choice overall seems to be partially connected.

The investigation into algorithm runtime presented in Figure 5.13 indicates that Hu (2019) [2] runs much slower that the other algorithms. While this is true for the MATLAB tests, the difference may be much smaller to the point that it is irrelevant in a real implementation. Therefore, the Hu (2019) [2] algorithm was not discarded from the comparisons.

To verify the calculated spectral effiency, the MIMO case was investigated. The achieved spectral efficiency for a single user system was found to be equal to the expected spectral efficiency in the case of CSI known at both receiver and transmitter, shown in Tse et al. (2005) [30, Eq. 8.40]. In the multi user case, the spectral efficiency was also found to agree with the expected spectral efficiency given in Spencer et al. (2004) [26, Eq. 13].

In the investigation of quantization of phase shifters, it was seen that the performance starts to slightly decrease below 4 control bits. Still, using 2 bit phase shifters seems to be quite effective here as well. This is promising for choosing low complexity components for a real system. These results are similar to the results found in Ayach (2014) [5].

It may be expected that the spectral efficiency should decrease drastically in the case of a large NMSE. Then, the weights are essentially calculated for one channel matrix but transmitted for another. However, the scattering environment is rich enough that while the signals are not transmitted in the optimal directions, some sub-optimal transmission still occurs. The investigated antenna arrays used in the

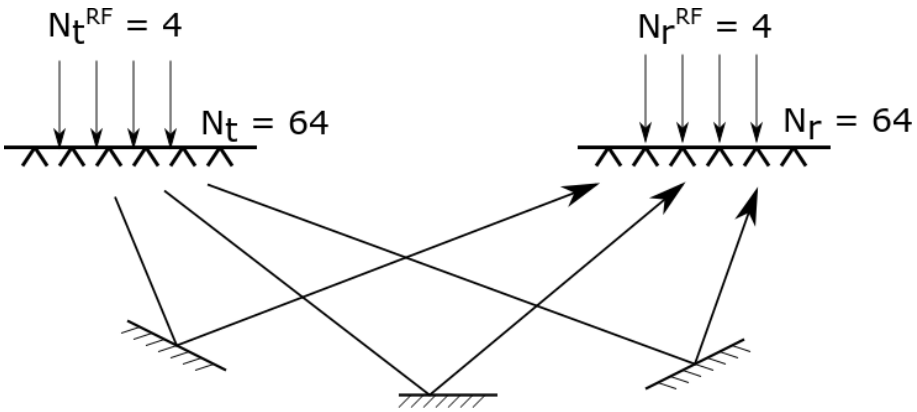

Figure 6.1: Proposed experiment setup with partially connected transmitter and receiver, in an environment with forced spatial diversity through reflectors.

error investigation have 8×8 and 4×4 elements. The half-power beamwidths (HPBW) were estimated using the `pattern` MATLAB function to roughly 16° and 28° respectively, in both elevation and azimuth direction due to the square arrays. Therefore, it's plausible that although the beams are directed somewhat wrong, some weak signal is still transferred.

6.3 Future Work

Channel estimation was judged to be outside the scope of this thesis, but it is a pressing issue that may limit the success of hybrid beamforming. Therefore, it is important to include in future work. An issue to get past is how to gain information about the antenna-to-antenna channel, when the signals from different antennas are combined before they reach digital processing. One thing to look towards may be to only sample the signal from one antenna at a time and go through the entire array. Another issue may be how often the channel needs to be refreshed; since the wavelength is so short, minor movements in the environment have a big impact on the channel.

In order to test the algorithms studied in this thesis, a hybrid beamforming system could be put together by combining several transceivers to work jointly. An example with 4 IQ channels for Tx and Rx respectively is considered. Each channel connects to an 8×2 antenna array through an FPGA which allows for phase shifting and amplitude control of the signal passed to each antenna. The system is then partially connected with 4 RF chains and in total 64 antennas.

Overall, the test setup would consist of two of these transceivers located nearby each other, kept at the same height but not necessarily facing each other. In order to improve channel diversity to enable spatial multiplexing, one suggested test setup is to turn the antenna arrays such that they face the same direction, then place several reflectors in front of them to allow several signal paths. This is shown in Figure 6.1. For this setup, only beamforming in the horizontal plane is done.

The investigated algorithms in Chapter 4 require knowledge of the channel, so the need for channel estimation becomes clear once more. If the channel matrix is not

completely known, it may be useful to start with the OMP algorithm since it is codebook based and the best entry can be selected by testing.

6.4 Relevance to Industry and Society

In order to meet increasing requirements on communication quality and to handle a growing amount of users, mm-wave communications will likely play an important role. Base stations capable of communication with multiple users at once maintaining high link quality at high frequencies are desirable [8]. In order to get to this point, hybrid beamforming seems to be a key element in finding a middle ground between cost and performance [8]. This thesis is therefore focused on an important area for realizing better connectivity in the future which will benefit society.
However, an increasingly connected society will also need to reduce the power consumption that comes with it. Evaluating power usage and comparing solutions based on it is therefore important. In this thesis, power consumption based analysis shows that sparsely connected RF architectures are preferable.
Striving for sustainability also means avoiding large, complex systems when possible. It's therefore critical to evaluate the necessary number of antennas and how much there is to gain from increasing system complexity. This thesis contributes with analysis of connectivity between RF chains and antennas. Finding the middle ground between simpler, partially connected systems and more complex but better performing fully connected systems can help to find a system that performs well enough but uses as few RF components as possible.

7
Conclusion

Hybrid beamforming was investigated for a variation of weight optimizing algorithms and RF architectures. Both single-user and multi-user cases were tested, as well as with one or multiple subcarriers. It was found through MATLAB simulations that:

- For a single user, a spectral efficiency of 22 bps/Hz was reached using hybrid beamforming with a fully connected RF architecture with an 8×8 transmit array and a 4×4 receiver array, at a transmit SNR of 0 dB. Spatial multiplexing was used to transmit 4 parallel data streams.
- Using a cluster based channel model with 16 clusters and 8 rays per cluster and the MIMO configuration described above, full MIMO had a slope of 4.3 bps/Hz/dB for SNR above 15 dB, but this was seen to be dependant on the number of clusters. Hybrid beamforming achieved a slope of 1.3 bps/Hz/dB.
- In the non-line-of-sight case, analog beamforming had a higher spectral efficiency than hybrid beamforming for SNR below -25 dB.
- In the case of line-of-sight with one multipath gain 20 dB stronger than the other, analog beamforming was better for an SNR below -10 dB. Here, the performance decreased for all algorithms with spatial multiplexing, due to decreased diversity.
- Adding quantization to phase shifters caused limited performance loss. It was negligible in the case of 4 bit quantization. For quantization with 2 bits, it caused a loss of about 14 % of the spectral efficiency without quantization.
- The number of antennas at the base station and the user equipment were varied. The spectral efficiency increased as much in either case for hybrid beamforming due to increased beamforming gain.
- Comparing the cluster based channel model against a generated channel based on measurements showed agreement between algorithm performance.
- The FPS algorithm [1] showed very poor power and hardware efficiency, while Wu (2018) [4] and Hu (2019) [2] performed best.
- The partially connected architectures had the highest efficiency referred to number of diodes and area. Some group connected configurations outperformed PC in terms of power efficiency.

Hybrid beamforming was shown to be a good candidate for future communication links. Multiple users and multiple subcarriers can be handled while maintaining a high spectral efficiency. While partially connected systems achieve a lower spectral efficiency, they are more efficient with resources and should be considered over fully connected architectures.

Bibliography

[1] X. Yu, J. Zhang, and K. B. Letaief, "A Hardware-Efficient Analog Network Structure for Hybrid Precoding in Millimeter Wave Systems", in *IEEE Journal on Selected Topics in Signal Processing*, vol. 12, Institute of Electrical and Electronics Engineers Inc., May 2018, pp. 282–297.

[2] C. Hu, Y. Liu, L. Liao, and R. Zhang, "Hybrid beamforming for multi-user MIMO with partially-connected RF architecture", *IET Communications*, vol. 13, no. 10, pp. 1356–1363, Jun. 2019.

[3] X. Yu, J. Zhang, and K. B. Letaief, "Alternating minimization for hybrid precoding in multiuser OFDM mmWave systems", in *2016 50th Asilomar Conference on Signals, Systems and Computers*, IEEE, Nov. 2016, pp. 281–285.

[4] X. Wu, D. Liu, and F. Yin, "Hybrid Beamforming for Multi-User Massive MIMO Systems", *IEEE Transactions on Communications*, vol. 66, no. 9, pp. 3879–3891, Sep. 2018.

[5] O. E. Ayach, S. Rajagopal, S. Abu-Surra, Z. Pi, and R. W. Heath, "Spatially sparse precoding in millimeter wave MIMO systems", *IEEE Transactions on Wireless Communications*, vol. 13, no. 3, pp. 1499–1513, 2014.

[6] A. Alkhateeb, G. Leus, and R. W. Heath, "Limited Feedback Hybrid Precoding for Multi-User Millimeter Wave Systems", *IEEE Transactions on Wireless Communications*, vol. 14, no. 11, pp. 6481–6494, Nov. 2015.

[7] X. Yu, J. C. Shen, J. Zhang, and K. B. Letaief, "Alternating Minimization Algorithms for Hybrid Precoding in Millimeter Wave MIMO Systems", in *IEEE Journal on Selected Topics in Signal Processing*, vol. 10, Institute of Electrical and Electronics Engineers Inc., Apr. 2016, pp. 485–500.

[8] I. Ahmed, S. Member, H. Khammari, A. Shahid, A. Musa, K. Soon Kim, E. De Poorter, and I. Moerman, "A Survey on Hybrid Beamforming Techniques in 5G: Architecture and System Model Perspectives", Tech. Rep., 2018.

[9] S. Mondal, R. Singh, A. I. Hussein, and J. Paramesh, "A 25-30 GHz Fully-Connected Hybrid Beamforming Receiver for MIMO Communication", *IEEE Journal of Solid-State Circuits*, vol. 53, no. 5, pp. 1275–1287, May 2018.

[10] H. T. Kim, B. S. Park, S. S. Song, T. S. Moon, S. H. Kim, J. M. Kim, J. Y. Chang, and Y. C. Ho, "A 28-GHz CMOS Direct Conversion Transceiver with Antenna Array for 5G Cellular System", *IEEE Journal of Solid-State Circuits*, vol. 53, no. 5, pp. 1245–1259, May 2018.

[11] H. T. Friis, "A Note on a Simple Transmission Formula", *Proceedings of the IRE*, vol. 34, no. 5, pp. 254–256, 1946.

[12] S. Geng and X. Zhao, "Feasibility Study of E-band mm-Wave for Gigabit point-to-point Wireless Communications", *Microwave and Optical Technology Letters*, vol. 55, no. 8, pp. 1969–1972, Aug. 2013.

[13] F. Fuschini, S. Häfner, M. Zoli, R. Müller, E. M. Vitucci, D. Dupleich, M. Barbiroli, J. Luo, E. Schulz, V. Degli-Esposti, and R. S. Thomä, "Item level characterization of mm-wave indoor propagation", *EURASIP Journal on Wireless Communications and Networking*, vol. 2016, no. 1, p. 4, Dec. 2016.

[14] H. Xie, "Sparse Channel Estimation in OFDM System", Tech. Rep.

[15] R. R. Romanofsky, "Array Phase Shifters: Theory and Technology", Tech. Rep., 2007.

[16] D. Zhang, Y. Wang, X. Li, and W. Xiang, "Hybridly Connected Structure for Hybrid Beamforming in mmWave Massive MIMO Systems", *IEEE Transactions on Communications*, vol. 66, no. 2, pp. 662–674, Feb. 2018.

[17] Z. Feng, S. Fu, T. Ming, and D. Liu, "Multichannel Continuously Tunable Microwave Phase Shifter With Capability of Frequency Doubling", *IEEE Photonics Journal*, vol. 6, no. 1, Feb. 2014.

[18] J. Lee and M. Seo, "A miniaturized 28 GHz 4-bit phase shifter in 65 nm LP CMOS for multi-channel 5-G radios", *Microwave and Optical Technology Letters*, vol. 61, no. 2, pp. 381–385, Feb. 2019.

[19] F. Akbar and A. Mortazawi, "A Frequency Tunable 360° Analog CMOS Phase Shifter with an Adjustable Amplitude", *IEEE Transactions on Circuits and Systems II: Express Briefs*, vol. 64, no. 12, pp. 1427–1431, Dec. 2017.

[20] H. A. Ameen, K. Abdelmonem, M. A. Elgamal, M. A. Mousa, O. Hamada, Y. Zakaria, and M. A. Abdalla, "A 28GHz four-channel phased-array transceiver in 65-nm CMOS technology for 5G applications", *AEU - International Journal of Electronics and Communications*, vol. 98, pp. 19–28, 2019.

[21] P. Indirayanti and P. Reynaert, "A 32 GHz 20 dBm-PSAT transformer-based Doherty power amplifier for multi-Gb/s 5G applications in 28 nm bulk CMOS", in *Digest of Papers - IEEE Radio Frequency Integrated Circuits Symposium*, Institute of Electrical and Electronics Engineers Inc., Jul. 2017, pp. 45–48.

[22] W. Lee and S. Hong, "Low-loss and small-size 28 GHz CMOS SPDT switches using switched inductor", in *Digest of Papers - IEEE Radio Frequency Integrated Circuits Symposium*, vol. 2018-June, Institute of Electrical and Electronics Engineers Inc., Aug. 2018, pp. 148–151.

[23] C. E. Shannon, "Communication in the Presence of Noise Classic Paper", Tech. Rep., 1998.

[24] Mathworks, *Introduction to Hybrid Beamforming*. [Online]. Available: `https://se.mathworks.com/help/phased/examples/introduction-to-hybrid-beamforming.html`.

[25] NYU Wireless, *NYUSIM: The Open Source 5G Channel Model Simulator software*. 2019, pp. 1–42. [Online]. Available: `http://wireless.engineering.nyu.edu/5g-millimeter-wave-channel-modeling-software/`.

[26] Q. H. Spencer, A. L. Swindlehurst, and M. Haardt, "Zero-forcing methods for downlink spatial multiplexing in multiuser MIMO channels", *IEEE Transactions on Signal Processing*, vol. 52, no. 2, pp. 461–471, Feb. 2004.

[27] Z. Pi, "Optimal transmitter beamforming with per-antenna power constraints", in *IEEE International Conference on Communications*, IEEE, 2012, pp. 3779–3784.

[28] S. He, C. Qi, Y. Wu, and Y. Huang, "Energy-Efficient Transceiver Design for Hybrid Sub-Array Architecture MIMO Systems", *IEEE Access*, vol. 4, pp. 9895–9905, 2016.

[29] M. K. Samimi and T. S. Rappaport, "3-D Millimeter-Wave Statistical Channel Model for 5G Wireless System Design", *IEEE Transactions on Microwave Theory and Techniques*, vol. 64, no. 7, pp. 2207–2225, 2016.

[30] D. Tse and P. Viswanath, *Fundamentals of Wireless Communication*. Cambridge University Press, May 2005.